Chapter 4
Some Methodological Foundations for Selecting and Processing AE Signals

Alongside the doubtless success of AE diagnostics of materials and structural elements, there is a number of methodical difficulties in applying this phenomenon. First of all, there is the problem of ensuring the reliability of AE results and comparing them with similar ones obtained in various laboratories and research centers. Such a situation can be explained by the lack of general methodical requirements concerning the AE testing of materials containing crack-like defects. To partly close this gap, in this chapter we generalize the approaches to AE estimation of crack growth resistance characteristics of materials, AE testing of products and structures, and others. Specific features of the AE investigations are related to the study of the AE and physico-mechanical processes. On the one hand, they should meet the requirements of fracture mechanics, and on the other [1], take into account the specificity of applying the AE method [2–4]. The greatest attention is given to the least investigated problems, such as the criterion for the selection of the AES generated by cracks among the signals emitted by other sources, the selection of the most informative AES parameters for crack examination, the selection of the AET operating frequency, and its location; some of these problems have been studied theoretically [5, 6]. Here we also focus on some other methodical aspects of the problem.

4.1 Some General Methodical Guidelines on the Use of the AE Method in the Mechanical Testing of Materials with Cracks

Note that there are no universal recommendations for AE investigations because they are performed in dissimilar conditions under the action of such factors as temperature, aggressive environment, loading, etc. However, it is possible to make

Z. Nazarchuk et al., *Acoustic Emission*, Foundations of Engineering Mechanics,
DOI 10.1007/978-3-319-49350-3_4

a certain systematization of the approaches by generalizing the known theoretical results and experiments' data.

In crack growth resistance testing of materials, the chart presented in Fig. 4.1 is most often used. The force *P*, created by a loading device 2, passes to a specimen 1 via a strain gauge. During propagation of macro-cracks in it, AET *4* and *5* receive the elastic waves, which are then passed on as an electric signal to a preamplifier *6* and afterwards to the block of filters *7*. The AES selected within a certain frequency band enter the coincidence block *8*, where they are subjected to spatial selection. The principle behind it consists of the following: the subsequent passage of the useful AE signal from AET *5* occurs only in the case when AES from AET *4* comes simultaneously to the coincidence unit *8*. Besides the AES filtration, this enables an additional elimination of the effect of mechanical noises on the results of AE research.

Next, the coincidence unit *8* opens the AE path (only in the case of the AES coincidence with AET *4*) and useful AES from AET *5* come to the block of data acquisition *9,* from which they can be selected for further processing and analysis.

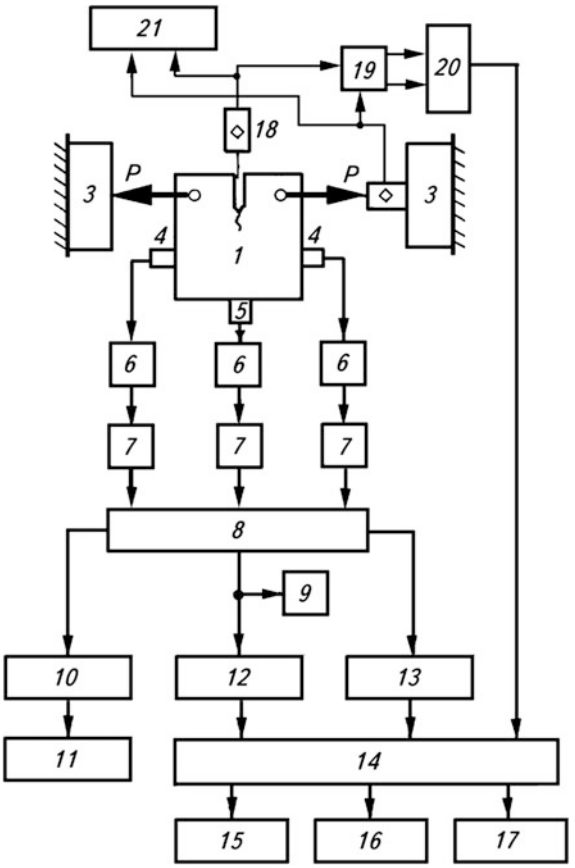

Fig. 4.1 Experimental testing setup

The AES can be simultaneously processed in an analog form by the simplest production run AE device *10* connected to the fast-acting recorder *11* of the required parameters. To obtain more complete information on a fracture, a fast-acting analog-to-digital converter (ADC) of AES *12* or spectrum analyzers *13* connected to personal computers *14* are used. Digital electric signals of loading forces can be supplied through the corresponding interfaces from a strain gauge *2* and crack opening displacement from the primary transducer of displacements *18*, which are preamplified by a two-channel measuring amplifier *19* and are converted into digits by a respective ADC *20*. A fracture diagram in the coordinates "*P* load—crack opening displacement *v*" can be recorded separately on a graph plotter *21*. Other necessary information is reproduced by peripheral devices *15* (monitor), *16* (digital graph plotter), and *17* (printer).

This setup may be either more complicated or simpler, depending on the experiments' tasks and on the available facilities and equipment. For example, channels for AE recording can be added in order to evaluate the emission source coordinates; a waveguide of the AE signals [7–9] may be applied for testing at temperatures different from the ambient or in an aggressive environment; and spectrum analyzers may be used to investigate the shape or the fine structure of the AE signals, etc.

Specimens and equipment are prepared for the experiments almost in the same way as for conventional crack growth resistance tests [1, 10–12]. Taking into account the above-mentioned, we present some basic ideas of this procedure. The primary AES transducer should have good acoustic contact with a specimen. For this purpose, the surface of a specimen is carefully treated in the location of mounting the AET. To improve the acoustic contact, appropriate auxiliary materials are used as a layer between AET and IO, and special techniques for fixing the AET upon the specimen are used [13, 14].

When preparing the equipment, at first the arrangement of a loading device is studied to predict the probable sources of external noises caused by the machine drives, friction in joints, and so on. Then the background hindrances are insulated from a specimen by anti-friction gaskets, appropriate joints, etc.

Preparation of specimens. The sizes of specimens and a method of their preparation are chosen, taking into consideration the specified tasks of an experiment: the type of a test, the loading mode, chamber size and geometry for making a required service environment and its parameters, type of the investigated material and its strength properties, structural features of loading devices, etc. Therefore, there are no general universally regulated methods of specimen manufacture and preparation for experimental researches. However, national standards determine some recommendations that consider the factors listed above. Thus, for instance, for a sheet metal that is 1–10 mm thick, it is recommended to use plane specimens, and for 20–100 mm thick, to use compact prismatic specimens subjected to eccentric tension [1]. In the 10–200 mm thickness range, prismatic specimens are used. For investigation purposes, cylindrical specimens are manufactured from round cross-section materials of 12–40 mm in diameter, and from bars of a square or rectangular cross-section up to 40 mm thick. Geometry and sizes of the specimens

cut out of the structural shapes, for example a T-section, channel and corner bars, pipes, etc., are chosen by considering the highest concentration of stresses and strains in the structural element of a certain type of rolling. In most cases for low- and medium-strength metals with a relative elongation of $\delta_5 \geq 15\%$ in three-point bending tests, the specimens that are simple in production and do not require large loadings during testing are used. In view of the strength properties of materials, the most universal are eccentric tension specimens.

When preparing specimens, the problem of choosing a specimen thickness or diameter arises. It is usually chosen considering the elasticity modulus E and the yield strength of a material σ_y, except for magnesium alloy specimens. Values of specimen thickness or diameter recommended for production are proposed in codes [1, 12, 15].

After choosing the specimen type, the specimen is mechanically processed to the required sizes, geometry and cleanness of the heat-treated surface. If such processing is complicated, a specimen is preliminarily manufactured with a tolerance not less than 0.5 mm, which is afterwards removed by polishing. Depending on the specimen type (milling, polishing, sawing through, etc.), electrochemical or mechanical methods are used to induce notches-concentrators of stresses. A fatigue crack is induced by the load that does not exceed 0.5 σ_y for stress ratio $R = 0.1\ldots 0.2$. For a cylindrical specimen under bending, $R = -1$.

It should be stressed that in preparing the specimens for AE research, it is important to prepare the place where the AET will be mounted. Most often it is prepared by mechanical or electrical polishing after grinding the specimen surface.

During specimen testing using the AE method at temperatures that differ from ambient, it is necessary to keep the requirements [1, 12, 15] of the corresponding codes dealing with test peculiarities. In cases of the AET mounted directly on the specimen, the waveguides of the AE signals are used, and AETs are affixed to them [16, 17].

Testing equipment. Application of the AE method to the research of strength characteristics of materials is related to certain requirements ascribed to testing machines and loading equipment. The basic requirement is a noiseless operation of the loading devices, since dynamic processes in a deformed material generate AE signals of insignificant power. If the minimum level of noises of such devices is not ensured, the information contained in AE signals can be lost in the background. Apart from noiseless operation, the loading machine should provide necessary forces and a loading law as well.

In the production-type testing machines, the hydraulic effects in servo-valves as well as operation of drives and friction in moving joints are potential sources of noise. For these reasons, many machines are not suitable for AE investigations in certain frequency ranges without an appropriate modernization. To this end, proceeding from the structural features of machines, the sources of noise should be revealed and removed. Thus, in designing the testing machines, the usage of hydraulic pumps with alternate motion should be avoided. To decrease the impact force phenomena under a pulsating loading, hydraulic accumulators are used, with their recharging pumps located outside the machine frame. In mechanical loading

devices, anti-friction gaskets and Teflon coatings are used to decrease the background noise caused by the friction of machine parts and units. Sometimes during loading, certain machine elements come into contact, thus generating low-frequency background noises in the range of 0.2–200 kHz. This greatly complicates the decoding of AE data, since these frequencies are often included in the operating range of an AE device. In order to provide isolation from such noises, special sound insulators are used that prevent the elastic pulses from reaching a specimen, or guide bearings are used to reduce the friction between the equipment units as much as possible [18]. An important factor causing a decrease of non-informative AE signals is the correct mounting of a specimen in the machine grips and the absence of plastic yielding of the material of a specimen in places where it gets into contact with the supports and grips. To improve the protection against the elastic background vibrations and electromagnetic waves, a machine or its operating part is placed in a special unit, and mineral fiber pads are placed between the connecting parts of a machine. These methods of protection against noises can be used for testing machines in AE investigations of structural materials.

However, even after modernization, many production-type machines are of little use for precise AE research. Therefore, machines with special loading devices have been designed for these investigations. They do not practically generate background noises [18]. There are also testing machines and equipment in which the noise reduction is accomplished by using a hand drive, vessels filled with water, thermal expansion and weight, etc., as a loading device. However, these devices have a few drawbacks; mechanical machines with a hand drive are low-powered and their application is limited. The devices in which the loading is created by the vessel weight gradually filled with water are used more frequently. The rest of the original devices used in the AE investigations do have a drawback: only simple loading laws are realized.

4.2 Technical Aspects of Preparation for AE Tests

Depending on the goal of the research, the available AE equipment [19–21] and the method of specimen testing, it is necessary to: (1) select the amplitude-frequency response of AET; (2) set the AE device operating frequency range that is outside the frequency band of the noise of loading devices; (3) set the threshold level and amplification factor of the AE path; and (4) calibrate the primary AE transducers by simulators. In Fig. 4.2, the simplest set-up for AE investigation of the crack growth resistance of structural steel specimens under three point bending is presented.

Recommendations for selecting the AET type, the method of its mounting on IO, and the provision of a reliable acoustic contact between the surfaces of a transducer and the investigated material were discussed earlier [22–24] and will be briefly discussed hereinafter. Therefore, here we discuss only the selection of the frequency band, the threshold level, and the amplification factor. The Kaiser effect is used for this in laboratory conditions under a repeated-static loading of the specimen without

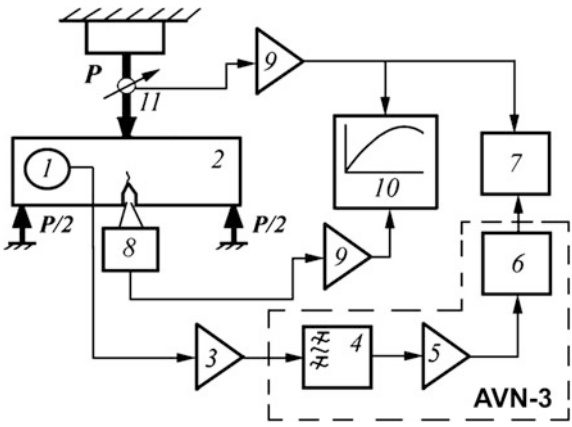

Fig. 4.2 Tensile testing of specimens with application of the AE phenomenon: *1* is the specimen; *2* is the primary transducer of displacement; *3* is the AET; *4* is the strain gauge; *5* is the loading device; *6* is the preamplifier; *7* is the block of filters of low and high frequencies; *8* is the power amplifier; *9* is blocks of the AES processing; *10* is the recording device; *11* is the amplifier of direct current; and *12* is the graph plotter

a crack by forces that exceed the critical values for a cracked specimen when the sub-critical crack growth begins. The specimen is loaded up to the values that exceed the critical load, and then it is unloaded and loaded again. Under a repeated loading, a lower frequency is selected, the threshold level is increased, and the amplification factor of a measuring path is optimized until the background noises vanish. In this case, the selection of the frequency band of noise filtration causes changes in the average amount of the AE pulses, which are acceptable [25].

During AE research, especially in the operating conditions, it is sometimes impossible to completely eliminate the background noises, whether mechanical, electric, or electromagnetic. Such noises can be part of the recorded AE data and can substantially complicate their decoding and interpretation, and in some cases can even lead to false conclusions. In this case, additional measures for the AE path protection are to be taken. For this purpose, in [26] a new effective method has been developed for the AE examination of cracks separating the AE signals from mechanical, electric, and electromagnetic noises. First, the remote zones of a specimen and the adjoining equipment are detected, where the highest values of the AE signal parameters from a crack and noises, respectively, are expected, and thus the difference between the arrival time of the signals from a noise zone is less than the AE event. The AETs with approximately identical amplitude-frequency response are mounted at these zones. The signals from these AETs arrive at two parallel similarly sensitive channels. The AES selection modes are set so that AE signals with almost similar amplitudes pass through the channels (or with a higher amplitude on the second channel than on the first because its transducer is closer to the noise area). During crack growth, when there are no noises, the AE signal passes through the first channel and is absent in the second (or much less than in the first one), which enables its selection on the AE diagram. Thus, the AES parameters caused by the crack growth are obtained by eliminating AES that are recorded simultaneously by all AE transducers with practically identical or somewhat higher amplitudes originated from the area of noise action (the second recording channel).

Before testing, it is helpful to preload a shunted specimen in a testing machine under a loading that exceeds the critical loading by 10…15% [27] in order to grind grips and reduce noise in them, i.e., application of the Kaiser effect. In testing, the AE data and load, displacements, etc., should be recorded synchronously and continuously. Depending on the purpose and experimental conditions, the recommendations and the type of loading can change.

To compare the results of the AE studies in various laboratories, it is necessary to know (1) the amplitude-frequency response of AET, its sensitivity and sensitivity of the whole AE system; (2) the operating frequency range of the system, the selected threshold level, the specimen material, and the geometry; (3) the AET location on the specimen and the method of its mounting; (4) the type of loading device, the method of holding a specimen in grips; and (5) the location of the loading device elements and the specimens, and so on.

4.3 Selection of Informative Parameters of AE Signals

As already mentioned, modern AE systems permit the recording and processing of many of the AES parameters: amplitude, pulse duration, frequency spectrum, number of pulses and events, change of these parameters in time, and others. However, the amplitude, count rate, and cumulative count of the AE signals are used most frequently. Using these parameters, the moment of the crack start and propagation were determined, enabling the evaluation of the corresponding stress intensity factors (SIF). Here, we will briefly discuss the key aspects of the problem.

Many researchers consider the possibility of establishing the moment of the crack start using the AE method. For this purpose, it is recommended to record the AES [28] appearance or a certain level attained by them. However, the first AE signals arise almost at the beginning of loading and they have small amplitudes [29], while the AES amplitudes and the cumulative count of AE depend on the device sensitivity, threshold level, and the selected frequency range [30]. All these prevent the researchers from obtaining reliable results.

During plastic deformation, the long-term and low amplitude AES are recorded, while during brittle fracture, short pulses with large amplitudes are recorded [31, 32]. The number of AE pulses is an integral characteristic depending on the signal amplitude and its duration. When the AES duration increases, the number of pulses recorded at a constant amplitude, in particular, using a resonance type of AET, also increases. Therefore, one can expect the appearance of AE signals with small amplitudes and a comparatively large cumulative count of AES. The initiation and propagation of micro- and macro-cracks will generate the AE signals with large amplitudes and a relatively small cumulative count.

These features are effectively used to detect the crack start and the AES identification from a propagating crack when there are only two mechanisms of the AE generation, i.e., plastic deformation and a macro-crack growth. However, in some

materials, additional AE sources appear, e.g., fracture of brittle inclusions or micro-crack formation. These processes can generate the AE signals that are often comparable by an amplitude with the AE signals caused by a macro-crack propagation that complicates the interpretation of AE diagrams and the evaluation of the crack length increment. In this case, the quantitative analysis of some amplitudes of AE signals is low-effective for evaluation of the crack start in materials that generate AES of considerable amplitudes under loading before the sub-critical crack propagation stage. Then it is essential to work out a criterion based on other AES parameters, such as the signal wave form, spectral features, etc., which would be effective for this situation.

4.4 Simulation of AE Sources

The methods of AE diagnostics provide a potential possibility of access and examination of the entire structures and buildings, for which it is very important to ensure a high level of integrity of elements, such as aircraft, bridges, pressure vessels, pipelines, etc. The sequence of events causing the AES that could be detected—namely, the processes of AE source formation, elastic wave propagation, transformation and processing of AE signals—is presented schematically in Fig. 4.3 [33]. It follows that in order to clearly determine the AE characteristics and thus identify the results obtained, it is very important to have the model AE sources for the AET verification and calibration of sensitivity of the whole AE path. In particular, the absence of such sources has caused an imperfect testing of materials and poor AE examination and diagnostics of structures for a long time.

A model source should possess the following characteristics [33]: repeatability, high reproducibility, and a well-established mechanism of a source action. These characteristics should be close to the real AE sources and relatively simple to be applied.

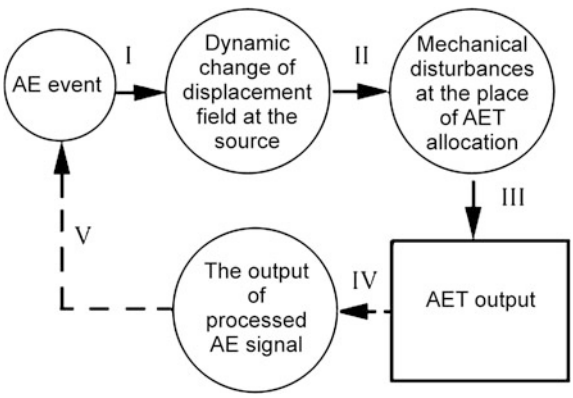

Fig. 4.3 Logical sequence of the AE event analysis: *I* is characteristic of the AE source; *II* is wave propagation in a solid; *III* is AET amplitude frequency response; *IV* is the AES processing; *V* is interpretation of AE data

Papers [34, 35] describe one of the first models of the AE sources, i.e., a source that is simulated by the failure of a glass capillary and satisfies, to a certain extent, the formulated requirements; this method of simulation was improved later [36]. A glass capillary was replaced by high-quality graphite lead, one end of which is pressed to the tested object with a constantly increasing pressurizing force until it fails. Thus, during fracture, the force of a stepwise function type is generated, and its value is chosen by adjusting the diameter and hardness of the lead. This simple method is accepted by the standardization groups of AE research in the U.S., Europe, and Japan as a standard method of AE verification and calibration of sensitivity of the channels of the AES selection and processing. The device with the lead provides a smooth loading and high reproduction of the shape of AE signals ensuring the process of absolute calibration.

Since the role of the AE source simulators in solving the problems of metrology prescriptions of the AE research facilities used for non-destructive testing of materials, products, and structures is very important, their development becomes very topical. Practical use of the AE source simulators shows that they also enable solving a number of additional problems related to optimizing the calibration of the AE facilities. Thus, simulators can be used for (1) checking the serviceability and adjustment of the channel sensitivity of AE devices; (2) recording the amplitude-frequency response of primary transducers and their directional diagrams; (3) evaluating the decay of AE signals and their propagation velocities in real constructions; (4) minimizing the measurement errors by the AET rational location and selection of its orientation; and (5) selecting the optimum frequency range and the threshold level of the AE signals, etc. [29].

The analysis of the published data shows that insufficient attention has been paid to the creation of the AE source simulators. Most of the researchers use different simulators with unknown technical characteristics; moreover, the principles of simulation have a number of drawbacks. The varying conditions of an acoustic contact between the AET and specimens result in low reproducibility of the AE signals, which are simulated and transmitted into the object tested. The mechanical resonance elements in the simulators lead to a misfit between the shape and the parameters of the simulated and real AE signals.

Some requirements for the AE source simulator result from the previously obtained characteristics of real signals: short duration, insignificant energy of a single pulse, high intensity, etc. (see Chap. 2). The amplitude of the mechanical displacement in the AE pulse can attain $10^{-7}\ldots10^{-14}$ m; a step-wise change in stresses in a source can take place within the small area of a square millimeter. It is also necessary to take into account the operating requirements of the AE application for the non-destructive testing of objects in special conditions. For instance, the quality control of welding during the formation of a weld requires the AE signals to be measured and simulated at high temperatures, and the presence of a corrosive environment or irradiation imposes special requirements for simulator stability or non-contact simulation. To decrease the AE research errors, it is necessary to provide a high reproducibility (stability) of signals induced by a simulator.

In practice, the simulators of the AE sources are based on the techniques of ultrasonic vibration excitation of a solid by a mechanical impact, reverse piezoelectric effect, magnetostriction transducer, spark discharge, or a light pulse. The analysis of these methods shows that none of them fully satisfies all the requirements [29].

When a solid—for instance, a ball—strikes the object under investigation, the mechanical vibrations that have ultrasonic components are excited in the object. However, to decrease the duration of a contact, it is necessary to increase the collision velocity that causes the growth of the energy of the excited vibrations. Calculations show that for the case of a steel ball with a diameter of 5.0 mm, the duration of a contact less than 100 μs occurs at a very-high collision velocity, yielding the energy of vibrations introduced in IO, which is not comparable with the AE.

The methods of vibration excitation by emitting AET based on a reverse piezoelectric effect consist of the following: AET eigenfrequency is chosen to lie within the frequency range of the AE excitation electric pulse. Then, AET emits a sequence of pulses, each of them being a decaying oscillation with a frequency equal to its resonance frequency. To avoid this phenomenon, it is necessary to increase the AET resonance eigenfrequency by applying very thin piezoelectric plates (for high frequencies). This complicates the sonic transmitter construction and deteriorates its reliability. One of the drawbacks of this method is a direct contact with the investigated object, a strong dependence of excitation efficiency on the quality, and the stability of a contact. The application of piezoelectric ceramics is limited by its relatively low values of the Curie temperature.

A magnetostriction transducer of the AE signals is widely used in experiments as well [37]. It is excited by the current pulses of 0.5 A, and duration of 3 μs with a frequency within 10 and 60 Hz. A waveguide in the form of a thin wire with basic resonance frequency of about 100 kHz is attached to the transducer that ends with a thin quenched point. Pulses excited in a waveguide in the form of longitudinal waves pass into the IO through the point pressed to it. The advantage of a simulator is the point area of transmitting the AE signals into IO and the possibility to simulate the AES at high temperatures. The disadvantage of the method is the necessity for an acoustic contact that reduces the reproducibility of the AE signals that are simulated and transmitted into the IO, and the presence of resonance elements. Therefore, a pulse duration increases, and it is impossible to adjust its shape. Besides, magnetostriction transducers effectively operate only at a frequency of up to 1 MHz, because the coefficient of transformation of the electric energy into the acoustic energy decreases proportionally to the frequency squared.

The electric discharge between the electrode and the surface of the IO is used as the AES simulator, which permits the formation of acoustic pulses of high power and short duration. According to data from the Dunegan/Endevco Company [38], a spark method is used for piezoelectric AET calibration. No information is given on the character and parameters of the AE pulses. Although the method actually provides the point introduction of vibrations, in the authors' opinion [29] it is still characterized by a low reproducibility of the elastic AE waves.

A method of acoustic wave excitation by a laser light pulse has its own advantages. Some modern solid lasers make it possible to get light bunches of power up to $10^{12}…10^{16}$ W/cm^2 with the simultaneous focusing of radiation in the spot of a diameter of 10…100 μm, creating rather powerful acoustic pulses. This method does not need an acoustic contact; therefore, it can be used for high-temperature, hard-to-reach objects. A light spot can be of virtually any configuration, such as point, narrow band, ring, etc. It is easy to inspect the amplitude of simulation pulses and their high stability. A drawback of this method is the short duration of a pulse in a single-pulse mode of irradiation and insufficient power of widely used lasers [29].

The fitting criterion of the simulation action of the AE source and a propagating defect is the identity of the elastic fields in close vicinity, where elastic waves are transmitted by a simulator. The fitting is established only by the parameters, which carry the information on the defect parameters. Instead of the above-mentioned criterion, it is possible to use the correspondence of the force or the kinematics effect of the simulator in the area of the vibrations input with the force or kinematical conditions on the simulated defect surface, assuming that the latter is on the input surface.

Some other methods of AES excitation in solids and liquids are also known [25, 28, 39, 40]. They use various physical principles of elastic wave generation and provide both discrete and continuous AES. These methods have both advantages and disadvantages and can be used in a laboratory and in production and field conditions of AE testing of materials and structures. However, progress in the research of crack growth resistance in structural materials, testing and diagnostics of products and constructions by the AE signals, brings up the problem of creating new, more perfect approaches to the simulation of AE signals in order to increase the reliability of the results, and consequently to provide the reliable operation of products and constructions.

Simulation of the AE source during evaluation of the static crack growth resistance of materials. Calibration of the instrumental AE path was done to compare the experimental results obtained by various authors in various research conditions. The methods of calibration of the AE channels turn out to be the most correct if the source of the AE simulation and AET are located directly on the IO. This is explained by the fact that the change of the place or the method of the AET mounting can substantially change the character of the response of the system "AET-IO" and thus affect the results of measurements.

In crack growth resistance testing of structural materials, it is important to provide a maximal sensitivity of the AE channel by calibration in order to reveal the early stages of sub-critical crack growth, and especially the moment of its start. It is known [5] that on the Mode I crack at the moment of its jump on the juvenile surface, an instantaneous decrease of stresses from the initial level to zero occurs; this is accompanied by the emission of elastic vibrations. Such single jumps of a crack very often provide a very small increment in the new surface area (for instance, for U8 steel it can be $(1.3…1.5) \times 10^{-9}$ m^2). As a result, the AE have low amplitudes of vibrations that propagate in a three-dimensional solid. Thus it follows

that we should not neglect the AE wave decay during precise AE measurements. It means that to simulate this decay in a solid, it is necessary to approach, as closely as possible, the real conditions of the elastic AE wave initiation and propagation in the material investigated.

It is shown [41] that the AE sources during crack propagation in a brittle body are mainly concentrated (about 70%) in the internal part of the specimen at a distance of 2 mm at both sides from the crack propagation plane. In this study, it is also shown that during a single crack jump in the body, the sequence of the arrival of AE elastic waves to AET is as follows: First, a longitudinal, then a transversal wave, then spatial waves reflected from the specimen surface, and, finally, surface waves arrive at the transducer. The AE vibrations that arose at the specimen surface continue with a greater amplitude than the vibrations excited inside the specimen (see also paper [42]). Therefore, the results of AE research will be more reliable if we model the AE signals from the internal part of a specimen near the probable plane of the crack growth with the fewest amplitudes and then perform calibration of the AE tools and AET by these signals. This is the purpose of the proposed model for the AE source simulation.

Thus, a glass capillary was used for the AE source simulation that maximally corresponds to a single crack jump. Glass, as the material for a brittle simulator, was chosen due to its homogeneity and isotropy. This permits, due to breaking the capillary, generating the same types of elastic waves with approximately identical characteristics of the AE signals. Figure 4.4 shows a capillary location in a compact [1] specimen *1* of the investigated material with an induced fatigue crack of a required length. A cylindrical hole, which nearly reaches the fatigue crack front, is made in the central part of the concentrator. A glass capillary *2* is inserted into the hole and clamped by a corresponding filler *3*. After preparing the specimen for testing, the AET is mounted on the specimen, and the AE signals from AET are transmitted electronically to the corresponding units of AE equipment. The AE path parameters, such as the amplification factor, threshold level of the AE signals, operating frequency band, etc., are selected by breaking the capillary with the AES recording. In this case, the optimum place for the AET location on the specimen surface is chosen [43].

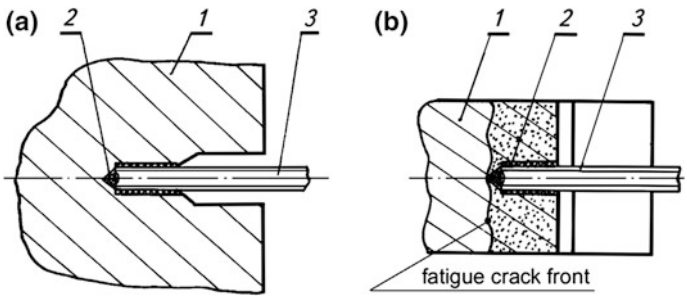

Fig. 4.4 Chart of a glass capillary clamping in the specimen body, vertical (**a**) and horizontal (**b**) axial cross-sections: *1* is a specimen, *2* is a capillary, *3* is a filler

Thus, when determining the static crack growth resistance of structural materials by the AE signals, the proposed method of the AE simulation eliminates the disadvantages of the AE source model proposed in [4]. The proposed method, in contrast to the one shown above, provides (1) a rigid clamping of the capillary end inside the specimen body that excludes its friction under loading; and (2) excitation of spatial waves that maximally represent the AE nature during a single crack jump with the minimum area of a fresh surface in the region of its most probable formation inside the material. The formation of the surface elastic Rayleigh and Lamb waves [44] is possible only if spatial waves are reflected from the specimen surfaces, thus permitting the reduction of their effect on the AE research results to the minimum by special measures [32].

Simulation of the AE source on the large-scale objects examined under field conditions. The application of the AE methods for non-destructive testing of industrial objects requires a very careful calibration of sensitivity of the measuring channels. This is an especially urgent problem, when the extent of the effect of the object geometry on the received AE signals, environmental effect, resonance of the object or the system "object-AET" are not well known. Quite often, when determining the AE source location on the object under investigation, some AETs have different sensitivities and respond ambiguously to some types of elastic waves, which cause an incorrect determination of the AE source and its orientation.

To interpret the results of measurements correctly and to compare them with the known verified or rated data and determine the degree of safe operation, it is necessary to simulate the AE sources of a high degree of repeatability with the approximation of crack-like defects propagation to the real conditions. Thus, the model of the AE source will be the more effective, the easier and simpler the simulation of the reproduction of AE signals in the conditions of detrimental effect of background noises that are plentiful in the industrial and field conditions of AE diagnostics.

It is known from the laboratory investigations [45] that pressure vessels and other constructions made of structural steel during sub-critical crack growth can generate the AE signals with the following gradation of their amplitude values: (1) weak AE signals caused by plastic deformation; (2) discrete AE signals with middle amplitudes caused by the fracture and/or separation of sulphide and silicide inclusions; and (3) the AE signals caused by the growth of a crack with wide-ranging amplitudes, depending on the local microstructure. Plastic deformation and fracture or separation of inclusions can arise during the formation of a plastic zone at the defect tip. Taking this into account, the simulation of AE signals consists of using the elastic waves emitted during crack propagation in the specimens made of the tested object material. By choosing the proper loading, and by measuring the crack length increment, it is possible to simulate various areas of fracture surfaces during an actual crack increment. This permits maximally approaching the real mechanisms of plastic zone formation and the stages of sub-critical growth of crack-like defects in the investigated object. Accordingly, having adjusted the AE equipment using the simulation of the AE sources, effective diagnostics and testing of objects by the AE signals can be performed [46].

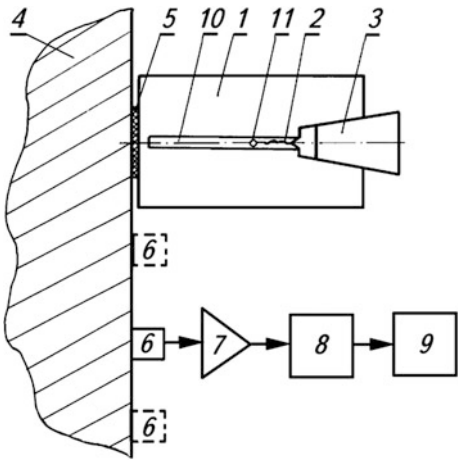

Fig. 4.5 Simulation of the AE source on IO permitting optimization of the AET location (schematically)

Figure 4.5 illustrates a scheme of the simulation process. Specimen *1* of the IO material in the form of a T-cantilever beam [47] with the preliminarily induced fatigue crack *2* is loaded to some calculated value *P*. Then, the loading is fixed on the specimen by a hard insertion *3* [48] and the specimen is mounted on the object *4* through a contact layer *5*. Specimen *1* is rigidly attached to the inspected object *4* by a threaded connection or gluing or soldering, etc., depending on the test conditions. At some distance from the specimen *1*, AET *6* is mounted, which is connected with a preamplifier *7* by a block of filtration and processing of the AE signals *8*, and with the recording device *9*.

The value of the loading force *P* should be calculated to prevent the propagation of the existing fatigue crack under a static loading by a rigid wedge. Catalysts are used to provoke its growth, i.e., the Rebinder effect [49]. When this happens, a crack begins to grow and move in the direction of the groove *10* to the hole *11*, which stops its further propagation, and plastic deformations appear at the hole due to the redistribution of mechanical stresses.

A repeated simulation on the same specimen permits selecting the service conditions of the AE facility, calibrating the AE sensitivity, and choosing the places of their optimum mounting with corrections for finding the coordinates and orientation of the AE sources. Thus, such an AE source simulation simplifies its excitation and maximally approximates the levels of signals to the real ones for different mechanisms of AE generation during propagation of the crack-like defects in the investigated object.

4.5 Simulation of AE Events at the AET Output

The methods for evaluating the AE path sensitivity of the facilities by excitation of the elastic AE waves, which arise and propagate in a solid and are received by AET, are described above. In some cases, in order to adjust the AE equipment units, it

seems promising to use the simulation of stochastic AES, which reproduce the sequence of the AE events that are expected at the AET output. The principle of the design and operation of such a device is described in [50].

The method of stochastic decimation of the Bernoulli sequence is realized in the simulator, which reproduces a stationary quasi-Poisson sequence of pulses with a given value of intensity of events or an exponentially decaying intensity of events. The initial intensity value m_0 and the parameter, time constant, T_0 of its decaying in time, are preset. The relative difference of dispersions of intervals between pulses at similar intensity of the flow of the AE events is a criterion of dissimilarity of a generating quasi-Poisson flow from the actual Poisson flow. The amplitude A_0 of the pulses can be regulated in a dynamic range of 10 dB, and their form at this stage is described by a cosine function with frequency ω exponentially decaying in time with the frequency ω. The parameter γ determines the exponential decay of this function, i.e., an informative component of the electric signal is generated in the form

$$A(t) = \sum_{i=0}^{\infty} A_0 \exp[-\gamma(t - t_i)] \cos[\omega(t - t_i)]\chi(t - t_i), \tag{4.1}$$

with distribution of the number of pulses in time

$$P(N) = \frac{\lambda^N}{N!} \mathrm{e}^{-\lambda}, \tag{4.2}$$

where

$$\lambda = \int_{t_0}^{t_0 + T} m(t)\mathrm{d}t, \quad m(t) = m_0$$

during generation of a stationary pulse flow of the AE events and

$$m(t) = m_0 \exp\left(-\frac{t - t_0}{T_0}\right)$$

during generation of a pulse flow with exponentially decaying intensity. Indicator function

$$\chi(t - t_i) = 1 \quad \text{if} \quad t \geq t_i, \quad \text{and} \quad \chi(t - t_i) = 0 \quad \text{if} \quad t < t_i.$$

The change in the value of the probability $p(t_j - t_0)$ of a pulse appearance for the simulator timing period according to the exponential law

$$p(t_j - t_0) = p_{\max} \exp\left(-\frac{t_j - t_0}{T_0}\right), \tag{4.3}$$

where $p_{\max}$ is the maximum value of probability of pulse appearance in a timing period, permits managing the value of the parameter T_0. The change of the clock period or clock frequency permits controlling the intensity m_0 of a stationary flow of the AE events.

A simulator (Fig. 4.6) consists of clock-pulse generator *1*, phase-pulse frequency dividers *2* and *3*, *S*-input 4, and three input elements of logical "and" 5, generator of the pseudo-random uniformly distributed binary numbers (GPUDBN) *6*, generator of digital exponent *7*, shaper of output pulses *8* and comparator of binary numbers *9*.

During each operation of a clock-pulse generator *1*, the next change of the pseudo-random uniformly distributed number at the outputs of the GPUDBN *6* occurs and *l* bits of this number are transmitted to the first inputs of a comparator circuit *9*, and other *s* positions are transmitted to the inputs of the logical element *4*. Pulse flow from the output of clock-pulse generator *1* through the frequency divider *2* with the division factor *k* is connected to the first input of logical element *5*, and through divider *3* with the division factor k_2 to the control input of the generator of digital exponent *7*. Under the control of the output pulses from divider *3*, the sequential output of values of *l* bit digital exponential function is transmitted from generator *7* to the second group of inputs of *l* bit comparator circuit *9*. Binary numbers are compared so that the potential of logical unit appears at the comparator circuit output only if the pseudo-random binary number is lower than the value of a digital function. The former of output pulses *8* sets the pulse amplitude, configuration, and polarity. In this case, configuration of the pulses is set by a pulse current impact excitation of an oscillating *RLC*-contour. To generate a stationary quasi-Poisson flow of pulses, the third input of element *5,* instead of the comparator circuit *9* output, is connected with the potential of a logical unit. Then, the value of intensity

$$m_0 = \frac{f_0}{2^s k}, \tag{4.4}$$

can be set by a corresponding switching of division factor *k* of frequency f_0.

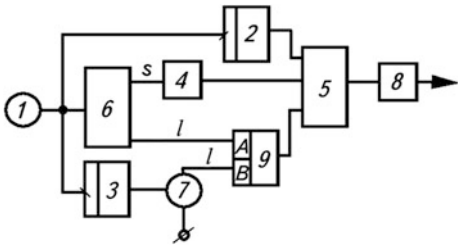

Fig. 4.6 Functional schemes of the simulator of AE events

The assigned exponential law of non-stationarity of the pulse flow intensity is introduced by setting a non-stationary digital function $Y(t)$. Since the sequential output of the function $Y(t)$ values is realized by the pulses of divider *3*, then by switching its division coefficient k_2, it is possible to adjust the rate of the change of the digital function, i.e., to compress or extend the specified functional dependence of the pulse flow intensity change in time.

The functional circuit of the digital exponent generator is shown in Fig. 4.7. It consists of $l + \alpha$-bit registers *1* and a subtraction circuit *2*. Its operation is organized so that from $(l + \alpha)$-bit number $Y(i - 1)$, the number $Y(i - 1)2^{-\alpha}$ is subtracted, i.e., the same number shifted by α digits to the right (in the direction of the least significant bits). Then, during the next recording of the result of subtraction in register *1* under control of the output pulse from divider 2 (Fig. 4.7), the number $Y_j = Y_{j-1} - Y_{j-1}\ 2^{-\alpha}$ will be recorded into register *1*, which is connected to the corresponding inputs of the comparator circuit. Thus, generator *7* produces an l-bit digital exponent.

$$Y(t) = Y_0 e^{-\frac{t}{T_0}} \tag{4.5}$$

The simulator of AE events is characterized by the following technical data:

- Intensity of the AE events flow $m_0 = (1, 2, 5) \cdot 10^a\ s^{-1}$ $(a = -1; 0; 1)$;
- Basic relative error of setting the intensity $\delta_{n_0} < 1\%$;
- Time constant $T_0 = 0.08 \cdot 2^b$ s $(q = 0, 1, 2, 3, 4, 5, 6)$;
- Relative error of setting the time constant T_0 of intensity decay $\delta_{T_0} < 1\%$;

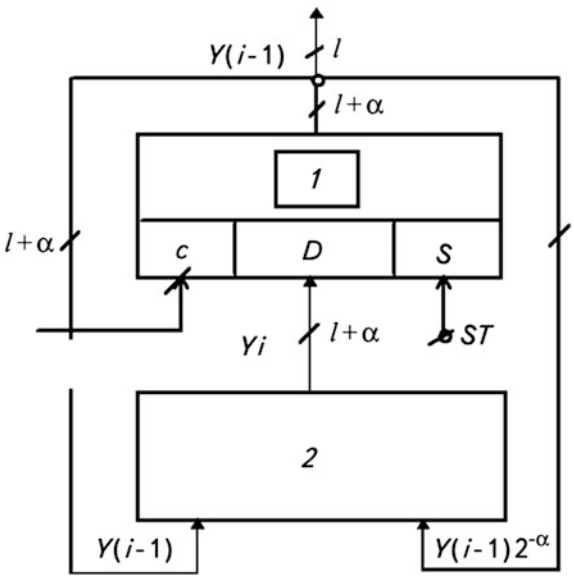

Fig. 4.7 Functional circuit of the digital exponent generator

- Difference of a generated flow from actual Poisson pulse sequence in terms of the criterion of relative difference of interval dispersions is less than or equal to 6%; and
- Initial pulses configuration of the simulator $F(t - t_i) = A_0\cos[\omega(t - t_1)]\exp[-\gamma(t - t_i)]$, $t \geq t_i$, where A_0 is regulated within the range of (0.2…2) V, ω = (0.3; 0.5; 1) MHz, $\gamma = (10^3; 10^4; 10^5)$ s^{-1}.

4.6 Spectrum of the AE Signals During Macro-crack Growth

The analysis of the AES spectra can provide important information on the stages of sub-critical crack propagation. On this basis, it is possible to build the criteria of assessing the state of structural elements or other products that contain crack-like defects [32, 51].

The theoretical investigations of the AES structure (including spectrum), have shown that the narrowing of the AES frequency band with the crack growth depends on SIF [5, 6]. According to calculations [52, 53], a frequency band can be of several megahertz, depending on the size of the defects. However, the operation of AE devices in the megahertz band is complicated for several technical reasons that can be often avoided: Experimental studies indicate that a frequency range lower than 4 MHz [54, 55] is sufficient for a crack inspection. Thus, the AES spectrum is in the range of up to 1 MHz, and an amplitude maximum of the frequency spectrum is at the frequency of less than 400 kHz [56]. Then, the results of the tests will only slightly depend on the type of material, AE transducer, specimen sizes, and the method of AES processing. However, it is known that the AES spectrum contains information not only on physical processes that generate AE; it also depends on the specimen geometry and size, as well as the characteristics of the AE transducers that substantially change the AES generated by a defect [40, 57–62].

Although the AES spectrum contains important information on the development of defects, sometimes the data contradict each other. Therefore a method was developed, and the AES structure was additionally investigated based on it—in particular their spectra during sub-critical crack propagation. In this way, an attempt was made to confirm theoretical predictions and technical recommendations on the choice of the operating frequency band of the primary AES transducer and AE equipment for diagnostics of the crack propagation stages and mechanisms.

Compact 1201-T 6 × 75 × 79 mm [51] aluminum alloy specimens were tested. A 35 mm long fatigue crack was initiated on the lateral edge of the specimen. Specimens were subjected to tension using a special SVR-5 device that provided smooth manual loading and the almost complete absence of background noises [18].

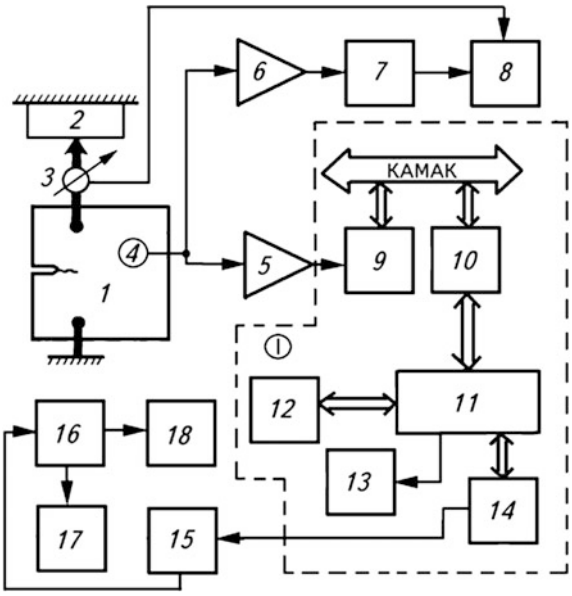

Fig. 4.8 A setup of the experimental research: *1* is a specimen; *2* is a loading device; *3* is a dynamometer; *4* is an AET; *5* is a preliminary amplifier; *6* is a measuring amplifier; *7* is an AE equipment AVN-3; *8* is a fast-acting recorder; *9* is an ADC; *10* is a dynamic set of the modules; *11* is a "MERA" computer; *12* is a processor of "Elecronika MT-70" equipment; *13* is a display; *14* is an E-256K quasi-disk; *15* is a translator-display; *16* is a computer; *17* is a monitor; and *18* is a printer

Available AE research equipment of the AF-15, AVN-3, and other types made it possible to get only the traditional parameters of AES (amplitude, power, duration, cumulative count, and count rate of the AES), but did not permit analyzing the fine AES structure, in particular their spectral distribution. Therefore, a specially designed informative measuring complex was used in the experiments [51] (Fig. 4.8).

The AET was used as an AE transducer. It is supplied with a set of AF–15 equipment with a pass band of 0.2…2.0 MHz and equal amplitude frequency response in the frequency range of 175…500 kHz. The AET was fixed by the clamp to the specimen through a contact layer of a lubricant. A block of two concatenated preamplifiers from the set of the AF-15 device served as a preliminary amplifier. The total amplification factor of the block was 70 dB, and a pass band was from 0.1 to 1.5 MHz.

The testing, selection, and processing of the AES were performed as follows: Under specimen loading, the crack grew, radiating elastic waves. These waves reached the lateral surface of the specimen and were transformed by AET into electrical signals, and then passed on for pre-amplification. From the amplification unit, the signals passed to the fast-acting F-4226 ADC with the main memory of 1 Kb permitting the storage of information that was transformed into a digital code

with the digitization frequency of 20 MHz. The period of internal timing was chosen in the range of 50–3200 ns. The digital sound, by sampling 1 Kb from the internal memory of ADC, was transmitted to the main memory of the fast-acting "Electronika MT-70" processor, where AES were functionally processed. The data array obtained was then transmitted to the memory of the "MERA" computer whereupon, through a display group of the "DYNAMO" AES modules, they were visualized on the screen. A total time of signal processing was less or equal to 1.5 s. Using the "MERA" computer, the information was recorded on a quasi-disk with a capacity of of 256 Kb, and then it was passed on to the PC memory via a translator. As an indicator, a channel was used that consisted of preamplifiers, an AVN-3 device, and an N-338/4 recorder, where amplitude, cumulative count of AES, and load were recorded. The AES was analyzed on different sections of the curve "Load P − crack opening displacement δ."

To obtain correct data from the experiment, at first the amplitude-frequency response of the "specimen-loading device-AET" system was investigated. For this purpose, a short-range AE pulse was used that was previously obtained for the linear section of the P-δ curve [51]. The spectrum of such a system had a wide frequency range of 2 MHz (Fig. 4.9).

For AES, as shown in Fig. 4.10a, the maximum irradiation is at the 630 kHz frequency. Taking into account the loading diagram, it is possible to assume that the signals recorded at the initial stages of a fracture diagram were caused by plastic deformations and micro-cracking at the crack tip.

Under further loading, a sub-critical crack growth affects the spectral characteristics of AES (Fig. 4.10b). Immediately after the crack start detected by an indicator channel, the frequency band of AE signals narrows jump-like to a frequency of 1 MHz and the spectrum maxima shifts towards the lower frequencies. For instance, the width of the frequency range (Fig. 4.10c) at the level of 0.7 of their maximal value, recorded at the middle stage of sub-critical crack growth, is 140…960 kHz. The narrowest frequency band at the point of deviation from linearity on the P-δ diagram (Fig. 4.10d) is only 90…530 kHz, and its maximum is at a frequency of 370 kHz. These AES correspond to the final stage of sub-critical

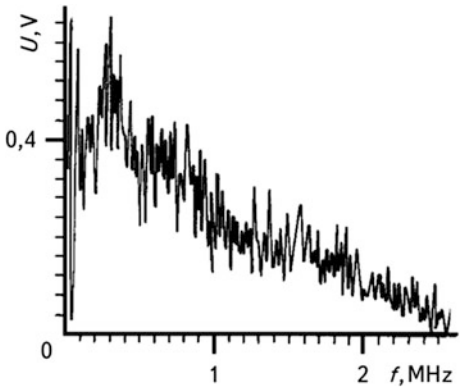

Fig. 4.9 AFC of the system "loading device-specimen—AET"

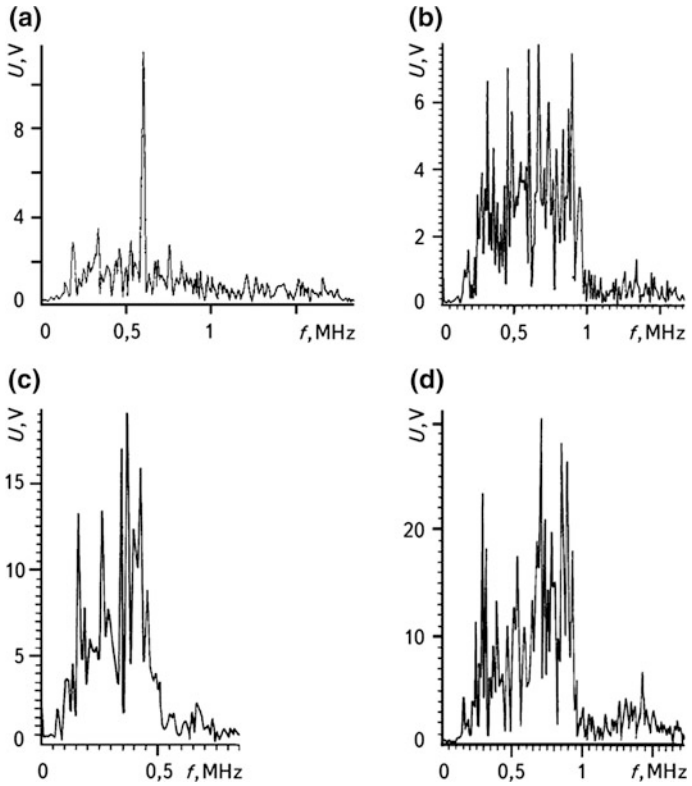

Fig. 4.10 The spectrum of AE signals at various loading stages: **a** on the linear section of the P-δ diagram; **b** at the initial stage of sub-critical crack growth; **c** at the middle stage; **d** at the final stage

crack growth. Thus, there are two important conclusions from the above-mentioned: Firstly, a jump-like narrowing of the frequency band can be used as a criterion for identifying the AES caused by the crack growth. Secondly, the narrow-band AE transducers having the resonance frequency band within 100… 600 kHz should be chosen. The low frequency limiting of the pass band is caused by significant noises of the loading devices at low frequencies.

As was theoretically predicted [5, 32], the width of the frequency band of AES at the stage of subcritical Mode I crack growth is inversely proportional to the SIF square

$$\Delta f = \beta K_I^2, \tag{4.6}$$

where $\beta = 0.25\ \alpha c_2/a\pi$; α is the proportionality factor; a is the material constant.

Theoretical predictions [63] (Fig. 4.11, solid line) concur with experimental data (dots) for the value of $\beta = 878.6$ (MPa)^{2}m/s. Thus, the width of the frequency band

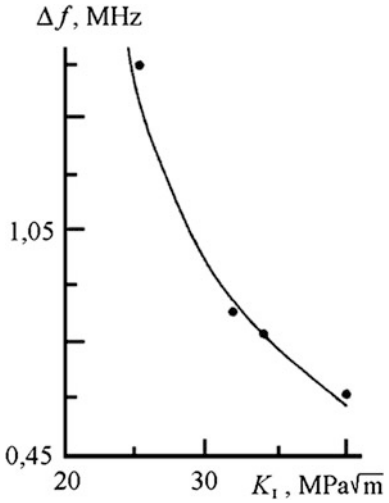

Fig. 4.11 Dependence of the frequency bandwidth of the AE signals Δf on SIF K_I at the stage of sub-critical crack growth

can be used for the SIF determination as well as for the calculation of a structural element strength under condition of its safe exploitation $K_I < 0.7\ K_{IC}$.

After crossing the highest point of the P-δ diagram, spreading of the frequency band, the shift of its maximum toward high frequencies, and an increase of the maxima by 2…3 times are caused—obviously by the fact that in the specimen at the overcritical stage, the crack propagates not in the initially induced crack plane, but in a curvilinear manner. As a result, the mechanism of crack propagation has changed from Mode I to Mode II fracture; this leads, as already mentioned, to the frequency band extension.

During the Mode II crack growth, it should be taken into consideration that the AE signals can be generated not only by overcritical crack propagation, but also by the friction of its faces. The AES with a wide frequency band and with maxima both at high and low frequencies, were detected up to the complete failure of the specimen. The width of the frequency band becomes the same as at the initial stages of sub-critical Mode I crack growth, but with the maxima larger by 2…3 times. The signals with a narrow frequency band were recorded among the AES with a wide frequency band, which means that at the overcritical stage, the crack develops due to various mechanisms. The indicator channel (with the use of the AVN-3 device) recorded the AES with large amplitudes.

The results were obtained using a certain investigative procedure (Fig. 4.8). When there is no indicator channel connected to the same AE transducer as the basic channel, the results can quantitatively differ to some extent. However, the main regularities established in this way should remain unchanged.

Figure 4.12 illustrates the frequency spectra obtained while evaluating the durability and static crack growth resistance of various materials.

Thus, with the start of sub-critical crack growth, the frequency band of AES narrows jump-like, which can be used as a criterion for the identification of AES caused by a crack. At the stage of sub-critical crack growth, as predicted

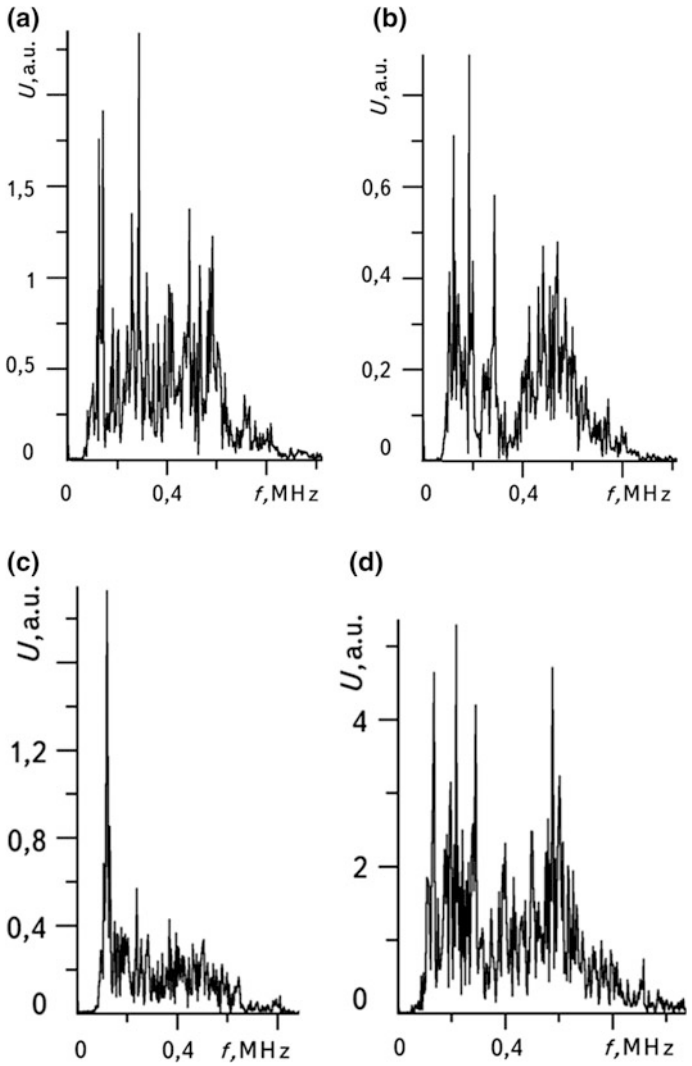

Fig. 4.12 The AES spectra at the initial (**a**, **b**) and final (**c**, **d**) stages of fracture of structural material specimens: **a** is the smooth cylindrical specimen of a diameter of 4 mm, steel 45, as delivered; **c** and **d** are prismatic precracked specimens of sizes 10 × 20 × 120 mm, 38XN3MFA steel, three-point bending

theoretically, the width of the frequency band is inversely proportional to the square of the stress intensity factor in the range of up to 1 MHz, and at final stages up to 600 kHz. With a crack transition to the overcritical stage, according to the Mode I–Mode II fracture, a frequency band extends and becomes approximately the same as at the initial stages of sub-critical crack growth. However, the frequency maxima differ by 2…3 times.

4.7 Directional Diagram of AE Radiation During Macro-crack Growth

The directional diagram of AE (DDAE), which is an angular distribution of the AES amplitudes, is very important for AE testing. Every AE source (crack, dislocation, cavity, etc.) has its inherent DDAE, which is related to the mechanism of the defect initiation or growth, its shape, and its type. When analyzing the DDAE, it is possible to develop certain technical recommendations on the most effective selection of AES and interpretation of the AE data obtained. Such recommendations, from the viewpoint of methodology, first of all concern the location of the AET with respect to the crack. For this, it is necessary to take into account the fact that a crack as a directed source has its own DDAE with maxima and minima [5]. On the other hand, AET, depending on their arrangement, can have different receiving directional diagrams and, consequently, there are directions of the highest and the lowest sensitivity of AES reception and detection [64]. Therefore, coordinating the radiation and reception diagrams by choosing the directions of mutual coincidence of their maxima, it is possible to increase the efficiency of AES detection and processing without taking additional measures.

At the stage of AE data interpretation using DDAE, the mechanism of crack formation, its sizes and orientation, defect type, and truth or falseness of the recorded AES can be established [65]. Below, after a short theoretical substantiation, there follows a description of an experimental method for determining the DDAE caused by a crack using serial AE devices.

The modern understanding of the acoustic radiation directivity is mainly based on theoretical investigations [65–68]. We will generalize some of them that deal with DDAE. First of all, we will pay attention to the investigations, where analytical dependencies for the DDAE calculation are obtained, simplifying the analysis and giving a visual pattern of the DDAE.

During the formation and development of a cavity, only one longitudinal wave emanates. Its directivity depends on the cavity's shape and on the mechanism of its formation or growth. If a cavity is a sphere in the center of radial tension, the radiation will be the same in all directions. In this case, the function of AE directivity, which describes DDAE, is $\Phi(\theta) = 1$ [29], where $OR\theta z$ is a spherical coordinate system. If a sphere-like cavity is in a solid under uni-axial tension, then the directivity of acoustic radiation appears, which is the angular dependence with respect to the plane of the crack location, and for a longitudinal wave, according to [68], $\Phi(\theta) = 1 - g\cos^2\theta$, where $g = 2(c_2/c_1)^2$. The same DDAE has a defect, which is a system of three mutually perpendicular dipoles or a penny-shaped Mode I crack [6, 63].

The theory of elastic waves radiation by a newly formed or sub-critical crack was presented in detail earlier [5, 6]; we will relate only to the results concerning DDAE. Formation of a Mode I or a Mode II crack in an infinite body excites not one but two types of waves—longitudinal and transversal. Consequently, if during AE testing only a longitudinal wave is detected, one can conclude that the defect is

a cavity rather than a crack. Identifying the cracks, one has to take into account that a Mode II crack generates one wave, which is transversal but not longitudinal.

DDAE is individual for every type of wave and depends on the mechanism of the crack formation (normal rupture, longitudinal, or transversal shear). For example, in the far-zone, the DDAE radiation is described for a Mode I crack by the following functions [69]:

- longitudinal wave

$$\Phi(\theta) = 1 - g\cos^2\theta, \tag{4.7}$$

- transversal wave

$$\Phi(\theta) = \sin^2\theta, \tag{4.8}$$

where angle $\theta = 0$ in the polar coordinates $Or\theta$ corresponds to the plane of the crack location. Note that in dependencies (4.7, 4.8), only the function of AE directivity is presented, and the proportionality factors, used in expressions for calculation of amplitudes, are omitted.

In the case of a crack jump of a half-disk shape, the function of AE directivity of a longitudinal wave is [63]

$$\Phi(\eta,\theta) = (1 - 2\varepsilon^2\cos^2\eta)(1 + \cos\eta_1)/[(1 + c_{R1}\cos\eta_1)D(-\cos\eta_1), \tag{4.9}$$

where

$$\cos\eta_1 = \cos\eta\left[\cos^2\eta + \sin^2\eta/\sin^2\theta\right]^{-1/2}; \quad \varepsilon = c_2/c_1; \quad c_{R1} = c_R/c_1;$$

$D(-\cos\eta_1)$ is integral, which is found numerically [70]; $OR\eta\theta$ are spherical coordinates. For a transversal wave in a half-space at the crack tip, this function can be written with sufficient accuracy as (4.8).

Comparison of dependencies (4.7)–(4.9) shows that DDAE depends on the mechanism of the defect initiation and growth, its shape, and its type. We can compare the theoretical results obtained according to formula (4.9) and by known experimental data [65, 71]. Note that in this study, the purposefully made wide-band and capacitance AE transducers, as well as the AE tools, were used, which permitted recording only a longitudinal wave in the band of several megahertz. Usually, resonance transducers are used for the AE tests. They do not permit separating longitudinal and transversal waves. In such a case, the recorded data represent a superposition of longitudinal and transversal waves, which is why it is imperative to investigate the DDAE that is the result of these two types of waves.

In paper [69], compact and disk-like 1201-T aluminum alloy specimens of of 120 mm in diameter and 12 mm thick, with a preliminarily induced fatigue edge crack, were tested for eccentric tension. Since theoretical results were obtained for an infinite body in order to compare them with the experimental ones, it is

necessary to decrease the reflection of waves from the specimen surfaces as much as possible. Therefore, in order to accelerate the decay of the reflected signals, the specimens were glued with the layers of rubber, which on one side had cuts for attaching the AE transducer.

AET were installed at various angles to the crack plane (0°, 30°, 45°, 60°, 90°), and the amplitudes of AES were recorded by five parallel channels. Each of the channels, except for the AE transducer, had a preliminary AE amplifier, AF-15 device, storage oscilloscope C8-12, and photographic recorder. The measurement conditions were: the pass band of the AE transducer was within 0.2…2.0 MHz with approximately identical amplitude-frequency response in the whole pass band, the amplification factor of the measuring path was 40 dB with the pass band within 0.2…1.0 MHz, and the transmission factor of filters was equal to 1.

Before being measured, the channels were calibrated receiving AES from the breakage of the graphite lead at the crack tip. Having adjusted the sensitivity of each channel, various levels of output signals were obtained, with the difference not exceeding 6%.

While testing the compact and disk specimens, the P-δ diagrams and AE diagrams were synchronously recorded (Fig. 4.13). By the cumulative count of the AE, N the moment of the crack start at the linear section of the P-δ diagram was determined. Three characteristic points corresponding to different stages of sub-critical crack growth were chosen for the analysis: Point I is the initial stage, Point II the final, and Point III the transitional, i.e., from sub-critical to over-critical propagation. Test results of compact and disk specimens show the similarity of the AES shapes recorded by each channel.

Angular distribution of the AES amplitudes (normalized to the amplitude that corresponds to an angle 0°) was calculated in the polar coordinate system (Fig. 4.14), assuming for an aluminum $\varepsilon = 0.266$ [66] and choosing the function of AE directivity from a condition $A = \max(A_1, A_2)$, where A_1 and A_2 are amplitudes

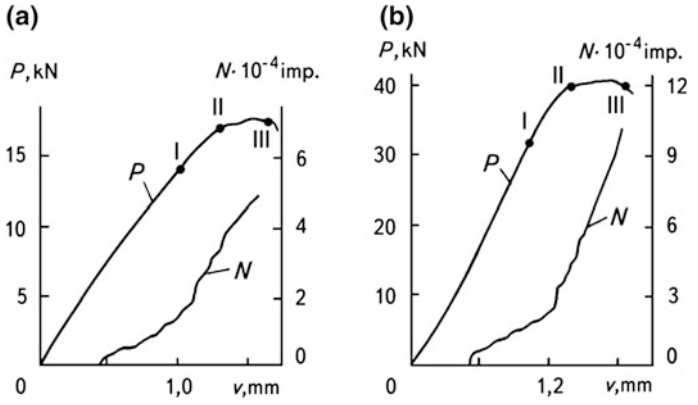

Fig. 4.13 Diagrams "load P − crack opening v" and the dependence of the AES cumulative count N change for compact (**a**) and disk specimens (**b**)

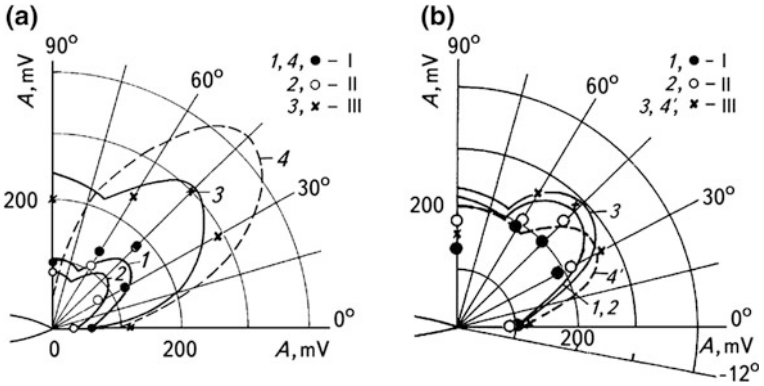

Fig. 4.14 Theoretical (*solid lines*) and experimental (*symbols*) DDAE for compact (**a**) and disk (**b**) specimens for different load values: curves *1*, *2*, *3* correspond to points I, II, III, respectively; *4* is DDAE for a dislocation rupture; *4′*—for a crack turned by an angle of 12°

of longitudinal and transversal waves, respectively, that were recorded by the channel. The DDAE type of each specimen is the same, i.e., AES were excited by the same defect—a sub-critically growing crack.

The agreement of theoretical and experimental data is better for a compact specimen. The ratio of the AES amplitudes, for example, for the angles 0, 45, and 90° is 1:3.5:2, respectively, and by theoretical calculations for a crack it is 1:2.8:2.1. If we assume that AES were caused by the plastic zone growth, the agreement is considerably worse. In fact, simulation of the plastic zone development by a dislocation rupture (constant jump of displacements on the fracture surface) according to Mode II fracture mechanism [72] at an angle of 45° to the plane of the crack location gives the ratio of the relative amplitudes 1:7.8:1 (dotted line in Fig. 4.14a). Theoretical results will substantially differ from experimental data if we consider that the basic source of the recorded AES is the plastic zone growth. Thus, one more criterion of identifying the AES caused by a crack and a plastic zone is the comparison of their DDAE.

For a disk specimen, theoretical and experimental results will differ somewhat, if we assume that the sub-critical crack grows in the plane of the preliminarily induced fatigue crack. Therefore, the angle defining the plane of crack propagation is recalculated. The analysis of the fracture surface showed that in a specimen, the crack propagates at an angle of 5°, while on a lateral surface at 30°. The best agreement of theoretical and experimental data is observed if the crack propagates at a 12° angle to the fatigue crack. Taking this into account, the DDAE is reconstructed (dotted line in Fig. 4.14b). Then, the ratio of theoretical and experimental values of amplitudes for angles 0, 45° and 90° is 1:2.2:1 and 1:2.4:1.5, respectively, which improves their correlation. Theoretical data also correctly coincide with the experimental results under cyclic loading of the 30XGSNA steel specimens [73].

The investigation of DDAE allows drawing a few conclusions and giving recommendations. Thus, the DDAE shape is affected by the mechanism of the defect

initiation or growth, its geometry, and its type. The proper selection of the optimum place of AE transducer mounting (by adjusting the defect DDAE with the receiving diagram of the AE transducer) increases the efficiency of AE tests. Using DDAE, it is possible to evaluate the crack length and orientation, the mechanism of its formation, and identify AES generated by the crack growth and other sources. As a result, a technical approach for the experimental evaluation of crack growth resistance of structural materials was developed. The main attention is paid to the least studied problems: methods of selection of the AES caused by a growing crack among signals caused by other sources, selection of the most effective parameters of AES for the crack detection, selection of the operating parameters of an AE device, and AE transducer location.

4.8 Estimation of AE Signals Caused by Propagation of Internal Crack-like Defects

A dynamic non-stationary problem on the instantaneous formation of a penny-shaped Mode I crack in the elastic homogeneous isotropic medium is investigated in [5, 6, 74]. It is assumed that the initiation of such a penny-shaped crack takes place when tensile stresses in some region inside the material attain a certain critical value σ_0. The appearance of the crack is modelled by an instantaneous fall of tensile stresses at the faces of the defects from initial level σ_0 to zero.

Based on the investigations of the first maxima of a displacement vector module for longitudinal and transversal waves at the observation angle θ ($\theta = \text{arctg}(z/r)$) in the range from 0 to $\pi/2$, and at distances from the observation point to a source larger than 30 crack radii, the following approximation expressions were proposed:

For a longitudinal wave

$$\Phi(\theta) = 1 - 2\varepsilon^2 \cos^2\theta\left(1 + \beta_1 \cos^2\theta\right)^{-1/2}, \tag{4.10}$$

and for a transversal wave

$$\Phi(\theta) = \left|\sin^2\theta\right|\left(1 + \beta_2 \cos^2\theta\right)^{-1/2}, \tag{4.11}$$

where $\beta_1 = 0.68$, $\beta_2 = 2.69$, and $\varepsilon = c_2/c_1$, which determine the angular distribution of radiation with an error less than 4%. Taking into account the dependencies (4.10) and (4.11) the following approximation fprmulas for evaluation of the maximal values of the displacement vector modulus were proposed:

$$\left|\vec{U}\right|_{\max|c_i} = \alpha_i \sigma_0 \Phi_i(\theta) r_0^2 \left(\rho c_1^2 R\right)^{-1} \quad (i = 1, 2), \tag{4.12}$$

where r_0 is the radius of a penny-shaped crack, R is the distance to the observation point, $i = 1$ corresponds to the longitudinal, and $i = 2$ to the transversal waves, $\alpha_1 = 0.452$, $\alpha_2 = 0.832$.

Dependencies (4.12) permit evaluating the size and orientation of a penny-shaped crack by the amplitude values of AES recorded by AET. For this purpose, at first the defect location should be found using the method of spatial location with four AET. Then, the procedure for finding the crack orientation is reduced to minimizing the following function:

$$F(\theta_0,\ \varphi_0) = \sum_{j=2}^{4} \left[\Gamma_j - \Phi_i(\alpha_j)/\Phi_i(\alpha_1)\right]^2, \tag{4.13}$$

where $\Gamma_k = \frac{A_k R_k}{A_1 R_1}$, $A_k(k = \overline{1,4})$ is the AE signal amplitude recorded by the k-th AET, which is considered to be proportional to the maximum of the displacement vector module determined by Eq. (4.13), R_k is the distance from the crack center to the k-th AET, the angles θ_0 and φ_0 are assigned in the spherical coordinate system $0R\theta\varphi$ with the origin that coincides with the crack center, α_j is the direction of the unit normal to the crack, functions $\Phi_i(\alpha_k)$ are determined by Eqs. (4.11) and (4.12), for longitudinal ($i = 1$) and transversal ($i = 2$) waves, respectively, $\alpha_k = \pi/2 - \theta_k$. Varying θ_0 in the range $[0, \pi/2]$, and φ_0—from 0 to 2π, for Γ_k being known from the experiment, and the values of functions $\Phi_i(\alpha_k)$ calculated according to (4.10) or (4.11) for longitudinal and transversal waves, respectively, we find a minimum $F(\theta_0, \phi_0)$ and the respective angles θ_0^* and ϕ_0^*, which determine the defect orientation that was sought. Using the dependence (4.4) for the known R_k, A_k, σ_0 and the crack orientation, we can calculate its radius.

To numerically verify the correctness and stability of the method proposed for the determination of a defect orientation by the AE signals, an error of ±20% was added to the values of Γ_k, which in general are determined experimentally, in comparison with their exact values found from Eq. (4.12), when we consider a certain case of mutual location of the crack and the AET system. According to Eq. (4.13) the error in determining the orientation angles θ_0^* and ϕ_0^* did not exceed 7%.

Investigating the AE radiation caused by sub-critical internal crack propagation in a material—in particular, in local regions near its front—is an important problem of AE diagnostics. To develop a corresponding model of the AE due to a small crack extension, an elastic body with a plane Mode I macro-crack bound by a smooth contour L was considered. A crack-like defect is formed under loading at some point in time, which is assumed to be initial in a small region near the crack contour where tensile stresses attain a critical value. Unloading its faces from an initial level to zero causes the emission of elastic waves that are recorded by AET. To simplify the problem, the formation of a penny-shaped Mode I crack of the same area at the macro-crack front is considered instead of a micro-defect. It is assumed that the radius to its contour is considerably smaller than the curvature radius of a plane macro-crack. Then, instead of the initial problem, there is a problem on the

displacement field caused by the sudden formation of a penny-shaped Mode I crack near a semi-infinite crack front.

An approximate solution to this problem in the spherical coordinate system $0R\theta\varphi$, whose center coincides with the center of a penny-shaped crack, is given as a product of the components of a displacement vector obtained from the solution to the problem on a penny-shaped crack formation [5, 6], and functions the $C_i(\alpha)$ that determine the effect of a semi-infinite crack-free surface on the angular distribution of emission in the form [70]:

$$\cos\alpha = (\cos\theta\sin\varphi + \delta)\left[(\cos\theta\sin\varphi + \delta)^2 + \sin^2\theta\right]^{-1/2}, \quad \delta = \Delta/R, \tag{4.14}$$

where c_R is the Rayleigh wave velocity, $K_-(\cdot)$ are the known functions,

$$\cos\alpha = (\cos\theta\sin\varphi + \delta)\left[(\cos\theta\sin\varphi + \delta)^2 + \sin^2\theta\right]^{-1/2}, \quad \delta = \Delta/R,$$

is the distance between the center of a penny-shaped crack and the tip of a semi-infinite crack.

Determination of orientation and size of a penny-shaped crack that formed near a semi-infinite crack front is evaluated by dependencies (4.13) taking into account the relationship (4.14). For a transversal wave, the angular dependence of radiation, due to the presence of a head wave in the region of angles α close to $\cos^{-1}(c_2/c_1)$, has a sharp maximum, which substantially complicates the determination of the defect orientation. Therefore, the advantage in AE investigations should be given to the reception of a longitudinal wave that is also used for the localization of the AES source by a triangulation method. The analysis of the displacement fields shows that the maximal values of displacement are proportional to the area of a new defect that is proved by experimental results [75, 76]. The angular distribution of radiation for a longitudinal wave in a plane $\varphi = 0$ shows that the AES amplitudes A caused by a micro-defect formation in front of the MC, can be determined by the following dependence:

$$A = \lambda S R^{-1}\Phi_1^d(\theta)C_1(\alpha), \tag{4.15}$$

where $\Phi_1^d(\theta)$ is evaluated from expression (4.10), and λ is the proportionality factor between an electric signal at the AET output and maximal displacement at the longitudinal wave front.

If during a sub-critical crack growth, M micro-cracks were formed, the total increment of a crack area will be

$$\Delta S = \sum_{k=1}^{M} s_k = \sum_{k=1}^{M} a_k A_k, \tag{4.16}$$

where

$$a_k = R_k / \left[\lambda \Phi_1^d(\theta_k) C_1(\alpha_k)\right].$$

The increment of a through-crack with a rectilinear front, when the formed defects go through the whole cross-section of a specimen (the cross-section thickness being equal to h), can be approximately evaluated by the formula

$$\Delta a = b/h \sum_{k=1}^{M} A_k, \tag{4.17}$$

where b is the constant to be evaluated from the experiment.

Investigating the free surface effect on AES caused by a penny-shaped crack, the surface displacements were sought as a product of the appropriate displacements obtained from the solution to a problem on the instantaneous formation of a penny-shaped Mode I crack in an elastic space, and the reflection coefficients. They were found in [77] from the approximate solution to the problem on a penny-shaped crack propagation in an elastic half-space within the framework of a ray theory in a wave front approximation. These displacements nearly coincide with the exact ones for the zone close to the epicenter on the condition that the crack radius is much smaller than the distance from its center to the half-space boundary. Using the performed calculations and the dependence (4.6), the following approximate formulas have been obtained for the maximal surface displacement values:

$$U^{(k)}_{\max|c_i} = \alpha_i \Phi_i(\theta) r_0^2 \left(\rho c_1^2 R\right)^{-1} R_1^{(k)}(\theta), \quad k = x, y; \tag{4.18}$$

where $R_i^{(k)}(\theta)$ are the reflection coefficients for longitudinal (i = 1) and transversal (i = 2) waves, respectively. Calculations made according to (4.18), have shown that for a longitudinal wave (Fig. 4.15a, b) the maximum values of the surface displacement in the epicenter almost twice exceed the respective values for an infinite body. For a transversal wave (Fig. 4.16c, d) at small distances from the epicenter, the character of the change in the surface displacement maximum is more complicated in comparison with a longitudinal wave. By combining formulas (4.15) and (4.18), we get a relationship:

$$A = \lambda S R^{-1} \Phi_1^d(\theta) C_1(\alpha) R_1^{(k)}(\theta), \tag{4.19}$$

that determines the AES amplitudes at the half-space surface caused by an incident longitudinal wave during sub-critical internal crack growth.

Dependencies (4.14) and (4.19) can be used to evaluate the sizes and orientation of the local fracture region by AES detected by the system of three AET that are located in the symmetry plane at a half-space boundary.

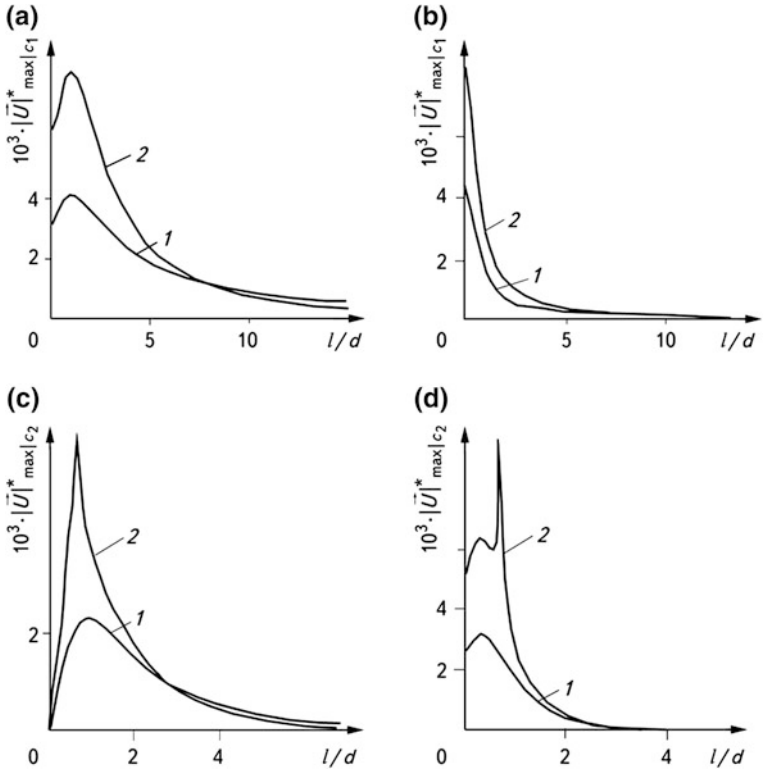

Fig. 4.15 Dependence of dimensionless value of the maximum of the displacement vector module at the surface of a half-space on dimensionless distance *l/d* for a longitudinal wave, $d/r_0 = 200$ for a longitudinal (**a**, **b**), and transversal (**c**, **d**) waves, the orientation angles $\eta = 0^o$ (**a**, **c**) and $\eta = 75^o$ (**b**, **d**): *1* is the incident wave, *2* is the total wave

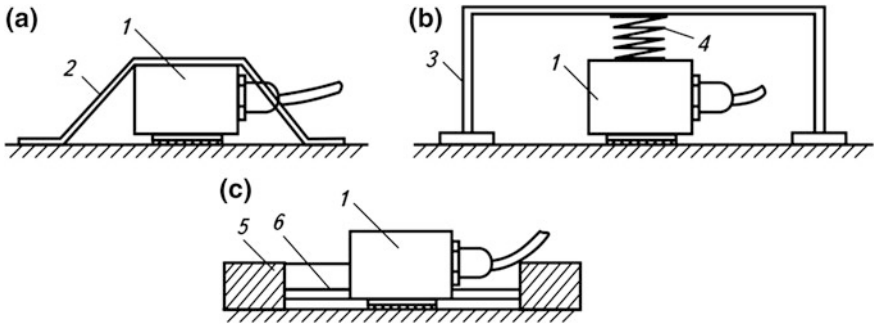

Fig. 4.16 Methods of the AET mounting on IO by adhesive tape (**a**), a spring (**b**), and a magnet (**c**): *1* is AET, *2* is adhesive tape, *3* is a spring, *4* is a carriage spring, *5* is a magnet, and *6* is a diaphragm

4.9 Methods of the AET Mounting at IO

Modern IO are characterized by a complicated geometrical shape, various physical properties of structural elements, service conditions, and the like. Therefore, the methods of the IO testing specify rigorous requirements to provide a reliable acoustic contact between IO and AET at the place of its mounting. In order to improve the contact between them, an intermediate acoustic transparent layer is used.

A thin intermediate layer between AET and solid IO can change the mechanical resonance frequency of the system and consequently decrease the resistance to wave propagation at the resonance frequency. This corresponds to an increase of mechanical quality factor, and to the narrowing of the band pass width of the system "AET-IO". The presence of a thin contact of acoustic transparent layer leads to an increase of the transmission factor by several times in comparison with a similar factor without the layer [78].

A wide range of techniques for mounting AET on IO are well known: methods using adhesive tapes (Fig. 4.16a), magnets (Fig. 4.16b), pressed springs with carriage springs (Fig. 4.16c), rubber vacuum chuck devices, etc. However, they cannot always be attached to IO due to their complicated shapes, low quality of surface treatment, physical peculiarities, etc. Besides, these methods do not always provide a reliable acoustic contact during product testing and do not ensure its stability in time. In addition, the devices for the AET mounting on IO with the application of magnets are as a rule rather bulky and inconvenient to use. Other facilities, in particular, fastening by an adhesive tape or gluing during deformation of the IO, frequently turn out to be the additional sources of noise and do not exclude the AET shift along the investigated object surface, although certain progress in the quality of the fastening is observed [14, 79].

Paper [80] describes the original device for the AET mounting on IO, which, being free from numerous disadvantages in traditional methods of mounting the AET, is still structurally complicated and bulky, and thus can be used only in some cases. The device (Fig. 4.17) consists of the AET *1,* connected to the AE

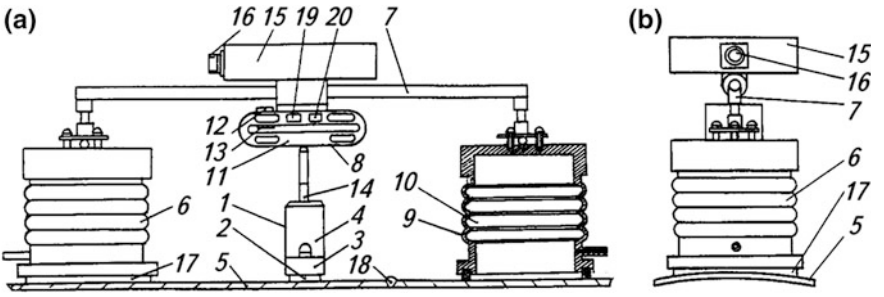

Fig. 4.17 Schematic of the device for the AES reception with a mechanism of mounting the AET on IO surface (**a**); side-view for testing the component with a curvilinear surface (**b**)

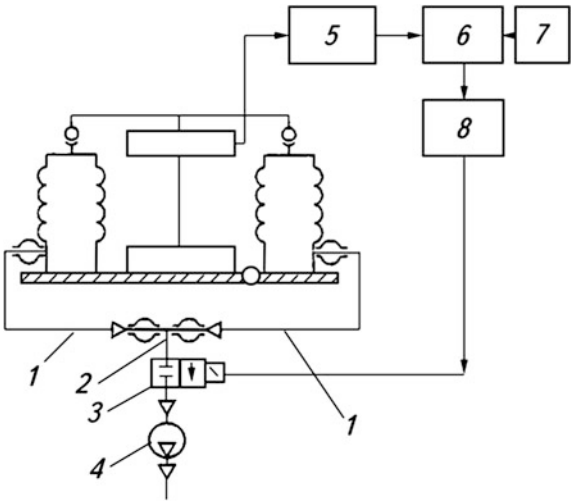

Fig. 4.18 Functional circuit of the AET holding mechanism control

waveguide 2 through the electro-acoustic transducer *3*, screening case *4* and the mechanism of the AET fastening to the IO surface 5. The mechanism for holding the AET *1* is manufactured in the form of vacuum chucks *6*, their number being determined by the IO geometry. The chucks are pivotally connected by beam *7*, which act through the pressing regulator *8* on the AET *1*. Vacuum chucks *6* are manufactured as bellows *9,* the cavities *10* of which are connected by tubes *1* (Fig. 4.18) to the vacuum pump *4*. Between tubes *1*, with the common nipple *2* and the vacuum pump *4*, there is a vacuum valve *3* with electromagnetic drive. Pressing regulator *8* (Fig. 4.17) is manufactured as an elastic element *11* with the strain sensors *12* and *13* fastened to it. The first one is located on the elastic element *11* from the side of the beam 7, and the second from the opposite side. The other side of elastic element *11* through the regulative element *14* interacts with AET *1*. Strain sensors *12* and *13* are plugged into an electric circuit that consists of a measuring amplifier *5* (Fig. 4.18), comparator *6,* force-control device *7,* relay *8* and vacuum valve *3* with electromagnetic drive, and a vacuum pump. Measuring amplifier *5,* comparator *6*, force-control device *7* and relay *8* are assembled into a common control unit *15* (Fig. 4.17), which through power socket *16*, is connected to the vacuum valve with an electromagnetic drive for sending commands. Bellows *9* have a ring gasket *17* located on the IO *5* surface with a weld joint *18*.

The device works as follows: Using a balance regulator, a measuring bridge of the pressing regulator *8* is adjusted. Regulating a force-control device *7*, a required pressing force of AET *1* to the IO *5* surface (Fig. 4.17) is found. A control unit *15* and vacuum pump *4* (Fig. 4.18) are turned on. The vacuum valve *3* with an electromagnetic drive is turned on through the normally closed contacts of relay *8*. As a result of pumping out and air decompression in the cavity *10* of the bellows *9* (Fig. 4.17), the latter get compressed. Through the beam *7*, the compressing force is transmitted to the pressing regulator *8*, regulating bar *14* and AET *1*. As a result,

deformation of the elastic element *11* occurs; it is transmitted to strain sensors *12* and *13*. The deformation of strain sensors results in the change of their electrical resistance value, which causes unbalancing of the bridge circuit; the unbalancing is increased by measuring amplifiers *5* (Fig. 4.18) and the increased voltage passes to comparator input 6. The comparator combines voltage of the amplifier and reference voltage from the force-control device *7*. When the voltage at the amplifier input *5* reaches the reference value, a positive voltage appears at the comparator output turning on the relay 8, which consequently turns off the power circuit of a vacuum valve *3* with an electromagnetic drive. As a result, a spring rod of the valve *3* closes the valve and stops pumping out the air from the cavities *10* of the bellows *9* (Fig. 4.17) by tubes *1* (Fig. 4.18).

An increase of air pressure in cavities *10* of bellows *9* (due to outside leakage) causes a reduction of pressing forces of the elastic element *11*, elastic deformation of resistors *12* and *13*, unbalance of the measuring bridge, turn-off of the comparator *6,* and turn-on of the vacuum valve *3* (Fig. 4.18) with the electromagnetic drive. The valve of the latter is turned on until a necessary force of pressing elastic element *11* is insured, and hence the AET *1* to the surface of IO *5* (Fig. 4.17). To remove the AET *1* from IO *5*, a vacuum pump 4 (Fig. 4.18) and control unit *15* are turned off and the air is let in by tubes into cavities *10* of bellows *9*.

The authors of paper [80] recommend using the device for AE diagnostics of welded joints in non-revolving joints of a large-diameter pipeline, storage, and petrochemical pressure vessels for the aviation industry, both during their use and their production. Such materials as austenitic steels, which are heat-resistant, heat-proof, cryogenic, etc., and titanium- and aluminum-based alloys, can be used for pipelines and vessels. This device is less effective in the NDT and technical diagnostics of cylindrical products with a small radius of curvature and with a considerable roughness of the IO surface. Thus, the correct use of the methods of the AET fastening to IO substantially increases the reliability of the AE test results that are obtained.

4.10 Selection of Useful AES During AE Tests

The experience of laboratory AE investigations and NDT of production objects [2, 9, 20, 24, 25, 29, 45, 51, 81] has shown that the most frequent difficulties in utilizing the AE phenomenon are related to the noises generated by the working devices, equipment, etc., and that it is hard to avoid their effect on the experiments' results. In most cases, various AE pseudo-signals can be observed: mechanical noises, such as friction in joints, vibrations, impact interaction of separate units, etc.; hydraulic noises conditioned by flow and leakage, boiling of working liquids; operation of power units etc., and electric interferences (internal thermal noises of devices, commutation of power machines and equipment, interferences of thyristor power control devices, and so on). Therefore, there is always a problem of reducing the IO noises not only related to the application of the measures described above,

(i.e., improving the loading machines and devices, calibration of sensitivity of the AE path for AES selection and processing, correct preparation of the operating place and the AET mounting, calibration of their sensitivity, application of parallel channels [82], etc.) but also in connection with the utilization of other technical approaches, the main of which are described below. Their practical realization is impossible without the previous detailed study of the parameters of noises generated in IO in real AE research conditions.

4.10.1 Selection of a Working Frequency Band of AE Facilities

Figure 4.19 schematically represents the AE elastic wave transformation during its propagation in IO from the AE source to the AET output which, having its own geometrical sizes, additionally (except for IO (Fig. 4.20b) modulates an elastic wave due to its amplitude-frequency response (Fig. 4.20b)).

In production conditions, a mechanical noise (MN) is the most widespread type of hindrance and they can have the greatest effect on the results of AE investigations. MN means elastic vibrations of the IO surface, which are not connected with the AE source action in the IO. Numerous experiments prove [25, 29, 32, 83, 84] that amplitude-frequency characteristics are conditioned by various mechanisms of their generation and can differ substantially (see Figs. 4.20, 4.21, 4.22, 4.23 and 4.24).

As seen in Fig. 4.20, a significant decrease in the MN effect during aerodynamic pipe operation can be expected at a frequency higher than 0.3 MHz [29], and the noise background of the working power reactor "Dresden 1" [83] is very weak, at a frequency higher than 0.5 MHz (Fig. 4.21). The MN of roller bearings depends on the available lubricant (Fig. 4.22) and has two typical frequency domains: in the range of 0.05…0.2 and 1.0….1.2 kHz [84], while the noise background of cyclic testing machines is limited by the frequency band of 0.002…0.3 MHz (Fig. 4.23) [29]. Mechanical loading devices have somewhat better noise characteristics in comparison with similar hydraulic machines for static loading (Fig. 4.24). The background noise, which accompanies the leakage of liquids and gases, has its own amplitude-frequency characteristics (see Figs. 4.25 and 4.26) [85].

Thus, when conducting the AE research, a number of questions arise in relation to the choice of the operating frequency band of AE equipment, taking into consideration the action of background noise. It is very important to determine the frequency spectrum of various kinds of noises generated by the equipment operating in its own or adjacent housing. Having generalized what was presented above, and the other known data from experiments [86, 87], it is possible to state that frequency characteristics of noise of various mechanical and hydraulic loading devices and vibration machines, as well as electric interferences, have particular frequency bands. The range of the frequency spectrum in MEN is 20…80 kHz, for

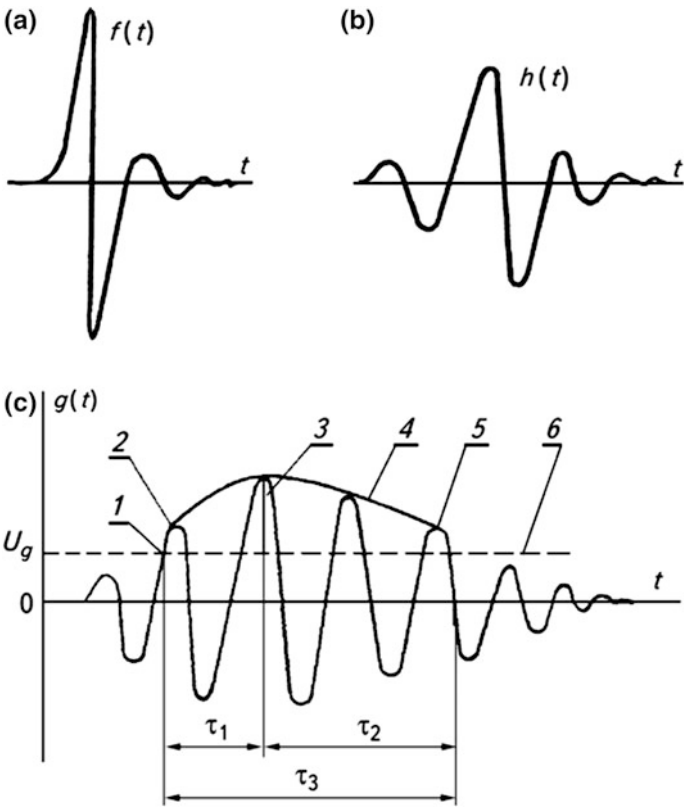

Fig. 4.19 Functions of the frequency distribution of the AE (**a**) event, response of the solid surface (**b**), and the AET (**c**): *1* is the moment of the AES arrival, *2* is the first pulse, *3* is the amplitude of an envelope curve, *4* is the envelope curve, *5* is the last pulse, τ_1 is the rise time of the wave front of the envelope curve, τ_2 is the time of decay, τ_3 is the duration of the event

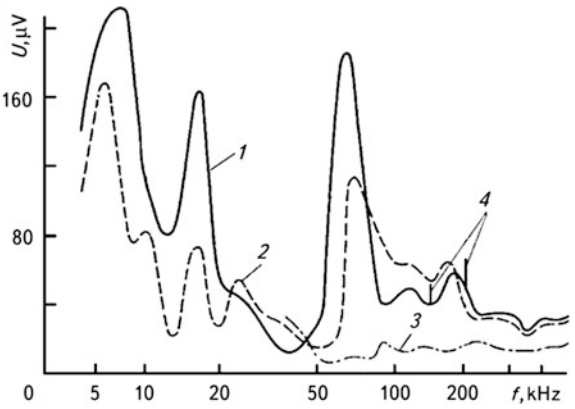

Fig. 4.20 MN spectra of the working aerodynamic pipe (the analyzed band of 1 kHz): *1* is normal service conditions with a model and a holder, *2* is without a model and a holder, *3* is the operation of ejectors only; resonance peaks of curve *1* at frequencies of 140 and 200 kHz are probably related to the conditions of a model and a holder streamline

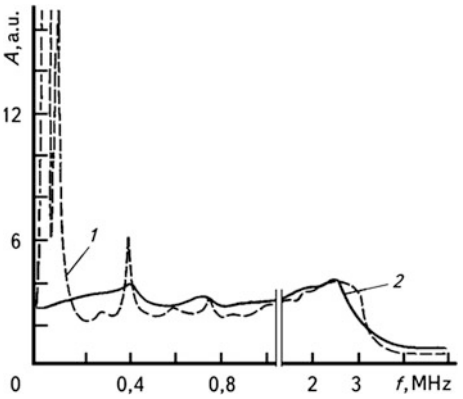

Fig. 4.21 Spectrum of noises of nuclear power reactor "Dresden-1": *1* is diameter of a circulating water collector of 560 mm; a flow speed is 7.6 m/s, high-pass filter (HPF) with a cut-off frequency of 20 kHz, amplification of 80 dB; *2* are noises of a testing system, with the AET placed on an external surface; amplification of 80 dB; HPF with a cut-off frequency of 20 kHz

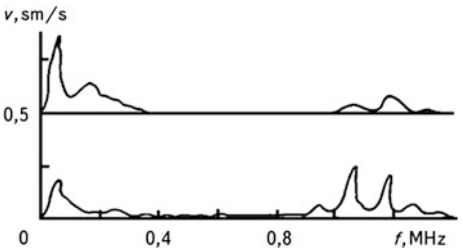

Fig. 4.22 Spectrogram of a roll bearing with the normal (*upper*) and insufficient lubrication (*v* is the speed of rotation)

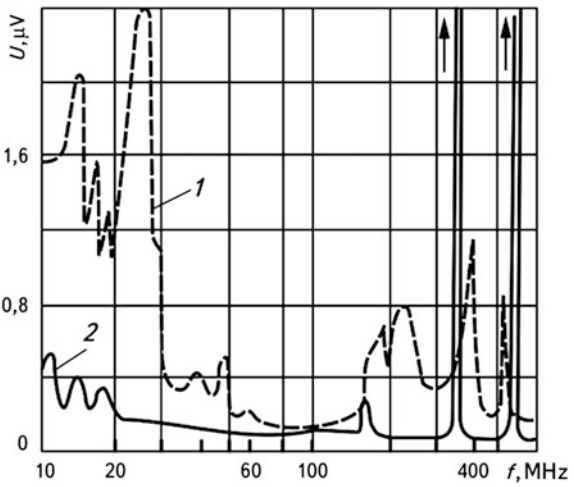

Fig. 4.23 Spectra of noises of testing machines (the analyzed band of 0.4 kHz): *1* is an electromechanical drive, and *2* is a hydraulic drive (frequency peaks at 340 and 590 kHz are electrical interferences)

hydraulic machines—20…400 kHz, and the vibration devices generate noises in the frequency band from dozens of Hz to several dozens of kHz. Electric interferences have the widest spectrum: from dozens of kHz to the units of MHz.

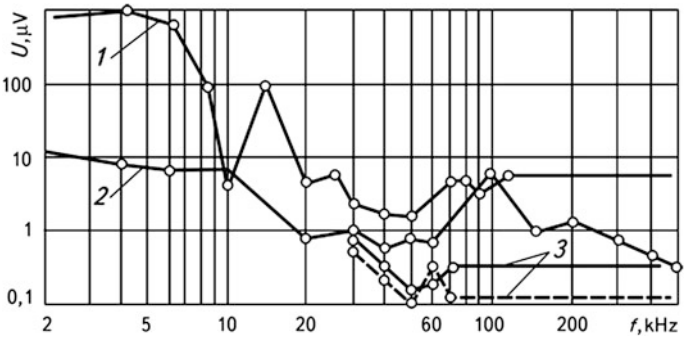

Fig. 4.24 Spectra of noises of cyclic loading testing machines (the analyzed band of 20 kHz): *1* is URM-2000, *2* is MUP-20, *3* is UMU-02 (mechanical drive)

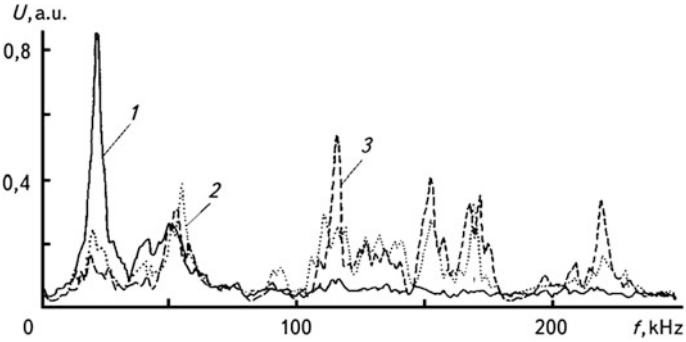

Fig. 4.25 The effect of backpressure P_0 on the spectrum of leakage noises in a hydraulic two-positional sleeve-valve at a flow pressure of 20 MPa: *1* $P_0 = 0$, efflux velocity $v_0 = 20$ ml/min; *2* $P_0 = 0.35$ MPa; $v_0 = 21$ ml/min; *3* $P_0 = 0.45$ MPa; $v_0 = 19.8$ ml/min

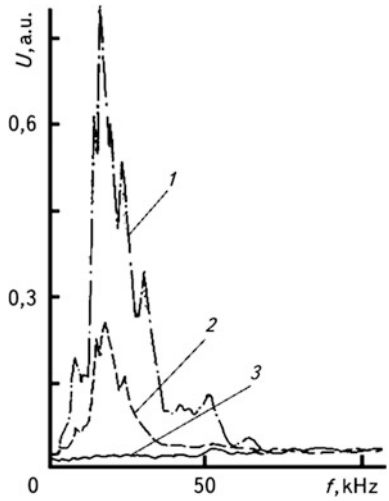

Fig. 4.26 Typical AE charts during leakage in a bullet valve of a diameter of 101.6 mm with the roughly treated layer and a new saddle: *1* is pressure drop ΔP − 0.072 MPa, efflux velocity $v_0 = 2000$ ml/min; *2* $\Delta P = 0.045$ MPa; $v_0 = 2000$ ml/min; *3* $\Delta P = 0$; $v_0 = 0$

Partly, methods for limitation of noise of all types consist of evaluating the level of discrimination (threshold level) of the AES selection over the level of noises (Fig. 4.19c) and in the selection of such a pass band of a device Δf where noises are the least (Fig. 4.27). As we can see, the radiation energy of noises in the range of high frequencies is low, and the change in the AE generation character does not substantially depend on the frequency range of its recording (Fig. 4.28). By selecting the appropriate values of the threshold level U_g and band pass of the AE device, it is possible to attain the best transmission of useful AES through the measuring path for their subsequent processing and recording.

In order to select the most appropriate operating frequency band of the AE device, it is necessary to take into account the frequency spectra of the AES which can radiate during the expected defect development. For instance, the method of

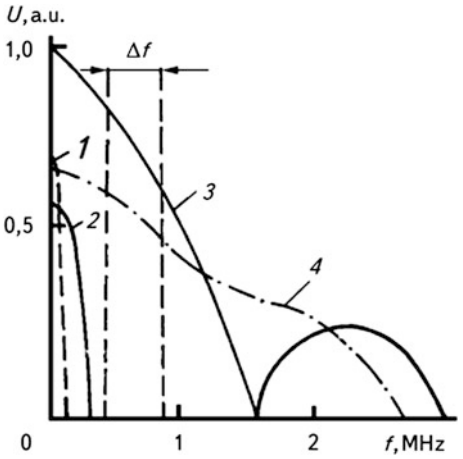

Fig. 4.27 Dependence of the noise spectrum amplitude on frequency: *1* are vibration machines, *2* are mechanical machines, *3* is leakage, and *4* are the AE useful signals

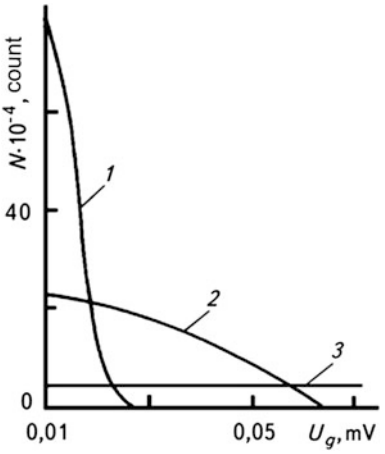

Fig. 4.28 Dependence of the mean value of the cumulative count of AES, *N*, on the level of discrimination and low cut-off frequency of the HPF: *1* for 360 kHz, *2* for 110, *3* for 11

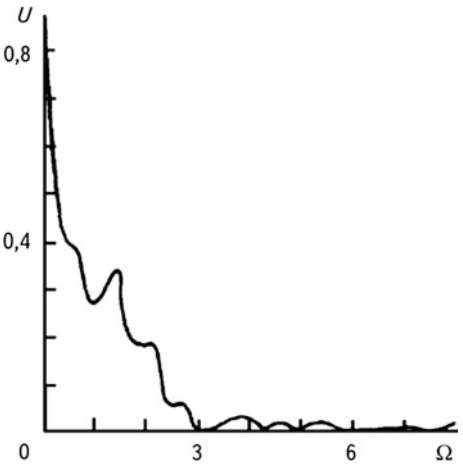

Fig. 4.29 Amplitude of the longitudinal wave frequency spectrum in the far-zone of radiation

preliminary theoretical estimation of the AES frequency spectrum, which can be generated during sub-critical jump-like crack propagation, is presented in paper [32]. It was modelled according to the formation of a penny-shaped flaw at the macro-crack front [5]. The solution to the corresponding dynamic problem of the crack theory made it possible to obtain a distribution of amplitudes shown in Fig. 4.29 in the frequency spectrum of the normalized displacement vector module.

Here, $\Omega = 2\pi f r_0/c_2$, where r_0 is the radius of a penny-shaped crack. As shown in Fig. 4.29, under the condition $U_0 \approx 0.7U$, the width of the main maximum $\Delta\Omega \approx 0.15$. If $c_2 \approx 3 \times 10^3$ m/s (for steel) and $r_0 = 2 \times 10^{-5}$ m, we get the frequency band $\Delta f = 0\ldots3.6$ MHz.

Some researchers, when investigating the initiation and development of materials failure, have experimentally determined the amplitude-frequency characteristics of AES. For example, it is shown in [88] that the AE radiation spectrum under mechanical testing of the welded specimen with a faulty fusion has specific features. The authors claim that AES can be identified by the amplitude and spectrum depending on a radiating source. Powerful AES during plastic deformation are recorded in the range of 0.8…3 MHz with maximal amplitude of about 0.06 V, when the micro-crack grows—0.35…1 MHz with amplitude to 0.15 V, and when the MC propagates—0.01…0.6 MHz with an amplitude up to 0.4 V.

The change of the frequency spectrum was also established experimentally in [56], where brass and steel specimens were tested. It was found that for these materials, the frequency spectrum is in the range of 0.1…1.0 ÌHz, and the most optimum operation frequency range is 0.15…0.3 MHz. We should note that the frequency spectra of AES are related to the mechanism of deformation, and the obtained investigation results do not depend on the material type, AET, specimen geometry, and the method of spectral analysis, although some areas of a frequency spectrum can be explained by the AES resonances that do not affect the main

frequency harmonics. The AES frequency spectrum in a brittle fracture of electronic chip ceramic substrates lies in the range of up to 10 MHz [89].

Thus, generalizing the above-mentioned, in order to optimize the width of the operating frequency band of AE device, it is necessary to take into account that the AES frequency spectrum is wide-ranging: from units of Hz to dozens of MHz. However, for experimental purposes, it is used as a rule within the range of 0.1… 2.0 MHz. Such a choice is conditioned by the fact that at lower frequencies, a high level of noise is revealed, while at high frequencies a strong decay of the AE waves is observed.

4.10.2 Filtration of AES by Instrumental Facilities

In the AE devices, the frequency range of input circuits is formed by setting the cut-off frequencies of filters, taking into account the selected operating frequency band and amplitude-frequency response of the AET. The width of the pass band is chosen by a low-cut filter (LCF) and HPF; the first one sets the upper limit, and the second sets the lower limit. Therefore, if the values—for instance 500 and 150 kHz —are set on them, this means that a pass band of measuring path frequencies is 150…500 kHz. In such devices, as a rule, the operating frequency band of the preamplifier is higher than the similar one in the amplification unit. Therefore, it is necessary to coordinate the pass-bands of its filters only. Hence, the filters should satisfy the following requirements [90]: (1) a high slope of the pass band cut-off; (2) a discrete adjustment by the choice of the upper and lower values of frequencies; and (3) avoid getting in resonance at cut-off frequencies.

It follows from the above that the frequency filtration of AES is an important link in the chain in the AE investigations and the key moments of its realization consist of the following sequence of measures:

- To preliminarily estimate the frequency spectrum of background noise of the working equipment that effects the IO;
- To preliminarily evaluate the amplitude-frequency characteristics of elastic wave radiation from the expected AE sources; and
- To choose an optimum pass band of filters, taking into account the frequency properties of the AET, noises, and useful AES.

4.10.3 Application of the "Dead Time" Mode

According to [29, 33], the AE signals can be classified as waves of a continuous shape, similar to "white noise," and as waves of a pulsating shape, i.e., pulses. The AES of the first type have a low energy level and many low-frequency components. They arise, as a rule, during plastic deformations. In the AES of a pulse,

i.e., in a discrete type of wave, the level of energy is high and the spectrum is characterized by high-frequency components. Such AES arise, for example, at a brittle fracture of materials. A proposed classification is conditional, because in the presence of a great number of discrete AE signals—for instance, at high rates of loading, when the time of their appearance is less than the duration of the AE event—it is very difficult to separate them. However, at slow jump-like sub-critical macro-crack growth [6], the signals originating from its jump-like propagation are well distinguished and are recorded as discrete AE.

In Fig. 4.30, the AE signal obtained at the AET output and its processing is represented schematically. It is clear that the selection of the AES threshold level affects the cumulative count and, consequently, the AE count rate. Therefore, during the noise cut-off, a certain error is introduced into the results of the AE research that is to be taken into account. Some methods of reducing the effect of such errors are known. For instance, the electronic units of the AES processing are

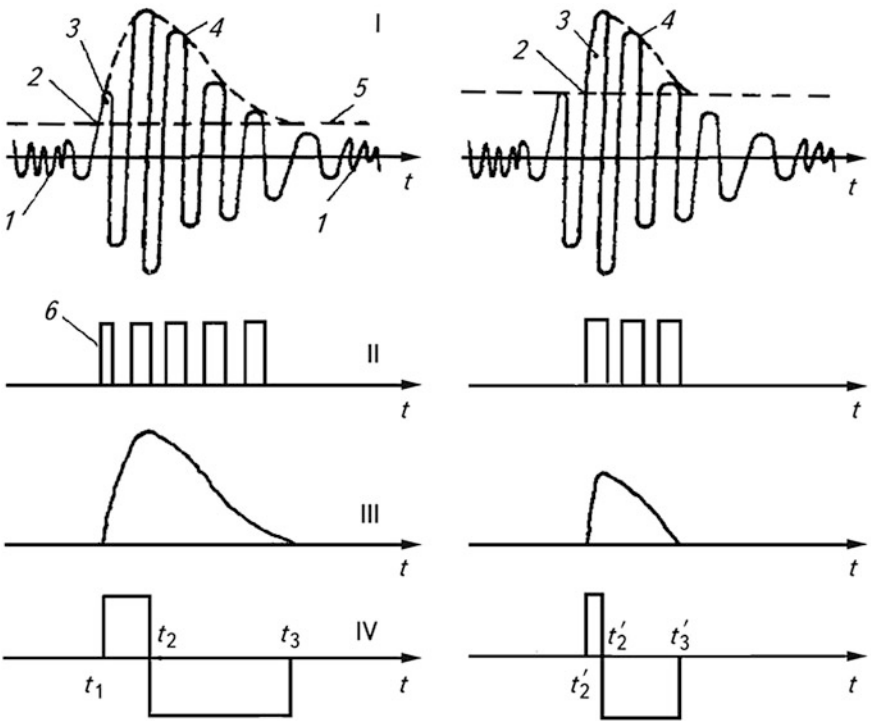

Fig. 4.30 AES processing by devices*: I* is the AE signal against the background noises; *II* is the count of pulses that exceed the threshold level; *III* is envelope selection; *IV* is formation of the "dead time" mode; *1* is a noise level, *2* is the moment that the count starts, *3* is the first pulse, *4* is the envelope level, *5* is the threshold level, *6* is the formation of the width of pulses by their duration; $t_1 - t_2\ \left(t_1^1 - t_2^1\right)$ is a period of time when an AE channel is open; $t_2 - t_3\ \left(t_2^1 - t_3^1\right)$ is when it is closed

adjusted to count the number of events that are estimated by the envelope curve formed by a peak detector (Fig. 4.30, Variant III) or the count is done by the first AE pulse obtained that exceeds the threshold level, and then the condition of "dead time" is applied (Fig. 4.30, variant 4). This, evidently, does not solve the problem of assessing the real number of counts (cumulative count of AE). However, the application of turn-off of the AE measuring path device for some time ("dead-time") enables us to distinguish spurious oscillations arising for these reasons. At first, the elastic AE waves that assist fracture due to the small specimen sizes are repeatedly reflected from its lateral surfaces, causing new types of elastic AE waves. All elastic waves, which are additionally excited in the specimen, are superposed and recorded by the AET. While applying the resonance AET, additional spurious vibrations caused by the resonance phenomena appear in the AET. In order to exclude their count from useful AES, an interval of "dead time" is used after the pulse reaches the threshold value of t_1 or t_1'.

When a certain threshold level for the selection of AES is specified, it is necessary to correctly choose the amplification factor of the AE path, which also affects the AES transmissions and their processing results. The amplification factor of the AE path is the sum of amplification factors in dB of the preamplifier and the measuring amplifier, i.e., the power amplifier. Our experience and the published data show that for ductile materials, the amplification factor can be of 90…120 dB, and in the case of brittle materials, it is up to 80 dB. The value of the amplification factor should be established separately for each case of the AE research.

4.10.4 The Kaiser Effect Application

In almost all cases of the AE investigations, the KE is used for reducing the noise effect and for specifying the threshold level. The essence of the approach consists of the following: During the repeated loadings at the level that does not exceed the previously reached value, the material is "noiseless," i.e., the AE recorded at the first loading is not observed (Fig. 4.31); thus, the material "memorizes" the load previously attained. For high-strength materials, such a "memory" is kept for a relatively long time. In low-carbon steels, especially at the elevated temperatures, it is possible to reduce the damage by annealing, and thus to regenerate the AE [91]. Hence, when adjusting the AE facility for noise protection, first the trial specimen without a crack is put in the grips or on the supports of the loading device, and stresses by 20…30% higher than the critical values for a similar cracked specimen are created in it. Then, the loading is gradually decreased—but not to zero—in order to avoid motions in grips or on supports, and after that the loading is increased again to the previously attained level. If no AES are recorded in this case, it means that there are no noise sources (i.e., friction at grips or at supports, noise from loading devices, etc.). In the case of the KE violation, it is necessary to use special clamps, sound insulation, and damping to eliminate this effect.

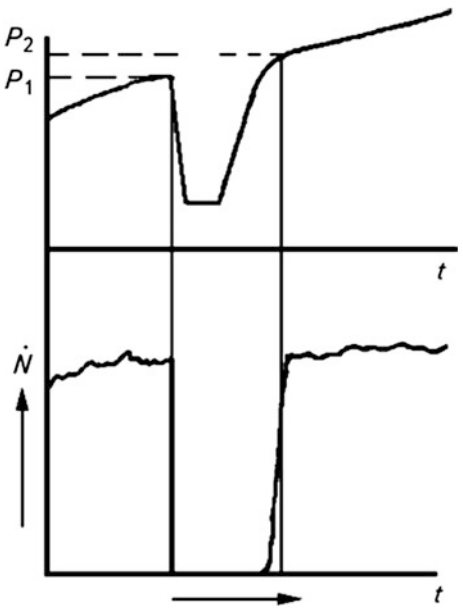

Fig. 4.31 Schematic of the KE implementation

At high levels of loading, the KE can be violated due to time-dependent processes, such as creeping. This is especially typical of the composite structures, where the KE disappears under the repeated loadings, which makes approximately 50% of a damaging failure load (the Felicity effect [4]). The KE does not hold during phase transformations, either.

Using the KE, the authors of [27] propose improving the reliability of the AE information obtained by the mechanical shunting of specimens before their testing. Shunts are mounted on the specimen's working part, and the specimen is loaded by a force that exceeds the damaging force. Thus, using the KE, the noises that would probably arise during loading in the elements of coupling, grips, and supports, are eliminated during their grinding to the specimen. Some technical approaches are known which, based on this effect, provide pressurization before testing the holes for the installation of the fingers of a loading device grip. For instance, a special device (Fig. 4.32) is used for this purpose in paper [92]. Similarly, it is possible to push the balls of a greater diameter and hardness through the specimen holes.

4.10.5 A Method of Spatial Selection of AES

To improve the reliability of the AE information obtained, the method of spatial selection is also used [93] (Fig. 4.33). Its essence is as follows: If AES 1 is first recorded by the auxiliary AET 3, and then by basic AET 4, this proves that the AE source is outside the inspected Zone I. A logical gating circuit of signal coincidence

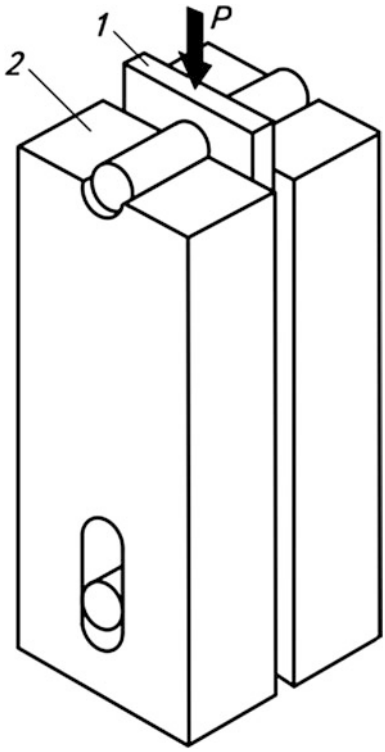

Fig. 4.32 Method of pressurizing the holes in a specimen by load *P*: *1* is the specimen, *2* is the support

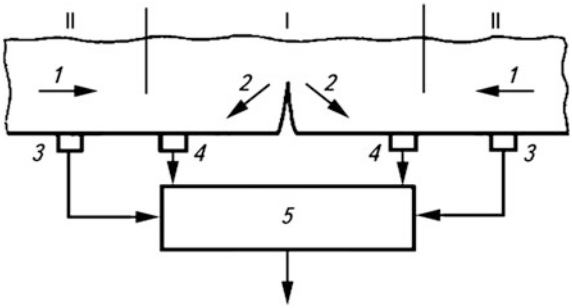

Fig. 4.33 A chart of the spatial selection method

5 in this case closes the input circuits of the AE devices and AES are not recorded. On the contrary, if at first AES 2 are recorded by PAE 4, the AE paths are open and AES are subsequently processed.

In paper [94], this method was modified: only AES reflected from the lateral surfaces of the specimen are recorded, which permits applying two arbitrary AET mounted on the specimen. The setups of spatial selection require the application of a computer technique, but at the same time they improve the reliability of AE information while investigating the material fracture. To increase the resistance of

large-scale objects to noise, a method of triangulation is used; this permits determining the AE source coordinates and thus improves the reliability of information.

4.10.6 Other Methodical Approaches

There are other methods for improving the noise resistance of the AE facilities and the reliability of the AE information. For instance, the AETs, which are sensitive only to a certain type of elastic waves or detect only a longitudinal spatial wave in IO, are used.

Under a cyclic loading, a part of MN within every cycle of loading is generated, where either useful signals are absent (friction of crack faces during the compression part of a cycle), or their amount is negligibly small. In such a case, an ordinary closing of input sections of the AE facility (time gating) in certain regions of a loading cycle eliminates the noise passing to the equipment.

In some AE facilities [95], in order to eliminate the noise effect on the AE results, setting a program-controlled selection of only those AES is foreseen; its time of growth of the forefront of the envelope curve is in the range assigned by an operator. Moreover, it is possible to determine the time of the envelope decrease, the time of the pulse after-effect, or to combine these values. Usually, in order to set the ranges of variation of these parameters, it is necessary to conduct the preliminary experiments on the IO material specimens.

It is well known [96] that even under uncertain selection of the AE equipment frequency range, the nature of the AES change during the tests is mainly the same. The authors validated this idea by testing standard 4340 10 mm thick steel compact specimens; these were subjected to tension with the parallel record of AES obtained from a low-frequency AET with the pass band of 2.0…20.0 kHz, and from a high-frequency AET with the pass band of 0.3…1.0 MHz. The AE information obtained is almost identical in both cases. The authors emphasize that the AES spectra do not depend on the specimen size, which concurs with the results of [56].

Summarizing what has been presented above, it is necessary to take into account the investigation results described in [33]. Using the results of the theoretical and experimental studies known at that time, the probabilistic scheme of defect detection in steels under loading up to the stress level of 500 MPa (Fig. 4.34) was synthesized therein.

Based on a review of a number of published sources, the authors proved that the AE method, compared with other known methods of non-destructive testing, is most sensitive to the detection of initiation and propagation of defects in a solid, and they emphasized that the threshold of detection in Fig. 4.34 in the laboratory testing is shifted substantially to the left, since in these conditions the least displacement at the IO surface, which is reliably recorded by the AET, is 10^{-14} m. The modern AE facilities make it possible to record the motion of single dislocations, fracture of carbides smaller than 1 μm in steels, lamination, or fracture of such

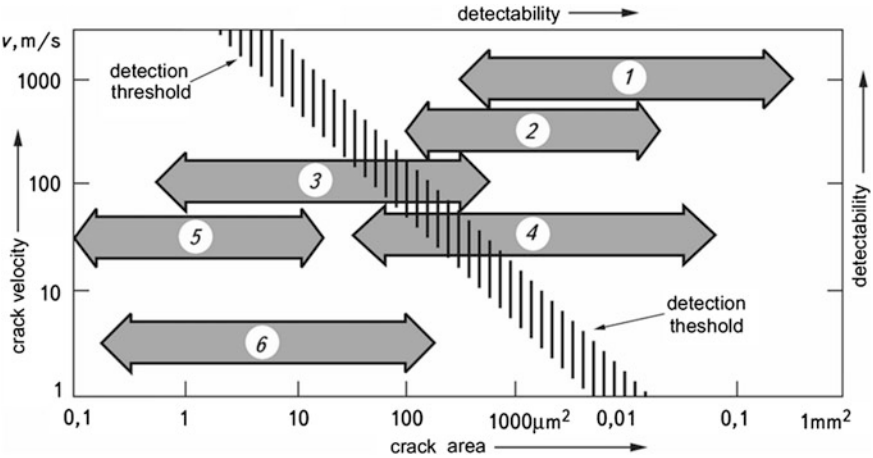

Fig. 4.34 Schematic distribution of the possibility of fracture detection in steels at different crack propagation rates v (the detection threshold corresponds to the AET sensitivity to the surface displacement of 10^{-13} m caused by a longitudinal wave; the distance between AET and the AE source is 0.1 m) *1* is the intergranular failure, *2* is the cleavage, *3* is the fracture of inclusions, *4* is the alternating shear, *5* is the fracture of carbides, *6* is the microvoid coalescence

inclusions as sulfides and silicides, initiation and coalescence of micropores, micro-cracks, etc.

Thus, there is a variety of methods for improving the noise resistance of the AE facilities. Their number grows steadily, and it is necessary to consider this and, therefore, to combine them in the AE studies. This will also enable correctly identifying the mechanisms of AES generation.

References

1. (1985) GOST 25.506–85. Raschety i ispytaniya na prochnost'. Metody mechanicheskich ispytaniy metallov. Opredelenie charakteristik treschinostoykosti (vyazkosti razrusheniya) pri staticheskom nagruzhenii. Vved. v deystvie 27.03.1985 g. (State Standard 25.506–85. Calculations and tests for strength. Methods of mechanical testing of materials. Determination of crack growth (fracture toughness) characteristics under static loading. Approved 27.03.1985). Izdatel'stvo standartov, Moskva
2. Ivanov VI, Belov IM (1981) Akustiko-emissionnyy kontrol' svarki i svarnych soedineniy (Acoustic emission monitoring of welding and welded joints). Mashinostroenie, Moskva
3. (1976) Standard recommended practice for acoustic emission monitoring of structures during controlled stimulation. ASTM E, pp 569–576
4. (1981) The EWAGE AE Code for acoustic emission examination of sources of discrete acoustic events. NDT Int 14(8):181–183
5. Andreykiv AY et al (1987) Teoreticheskie konzepzii metoda akusticheskoy emissii v issledovanii prozessov razrusheniya (Theoretical concepts of acoustic emission method in the

fracture processes investigations). Preprint, NAN Ukrayini, Fizyko-mechanichnyi instytut, 137(1987), L'viv
6. Andreykiv AY, Lysak MV (1989) Metod akusticheskoy emissii v issledovanii prozessov razrusheniya (A method of acoustic emission in investigation of fracture processes). Naukova Dumka, Kiev
7. Andreykiv OY, Lysak MV, Skalsky VR (1996) A method of accelerated evaluation of K_{ISCC} under stress corrosion cracking. Eng Fract Mech 54(3):387–394
8. Andreykiv AY et al (1992) Metodika opredeleniya K_{Iscc} stali v srede vodoroda s pomosch'yu metoda akusticheskoy emissii (A method of determining K_{Iscc} values of steel in hydrogen using acoustic emission). Tekhnicheskaia diagnostika i nerazrushyuschii kontrol (Tech Diagn Nondestr Test) 1:18–26
9. Andreykiv OY, Serhiyenko OM, Skalskyi VR (2001) Aktual'ni pytannya vidboru i peredachi signaliv akustichnoyi emisiyi pid chas rostu vnutrishnich trischyn (Actual problems of selection and transmissions of signals of acoustic emission during growth of internal cracks). Vidbir i obrobka informaziyi (Sel Process Inf) 15(91):51–59
10. Brown W, Srawley J (1972) Ispytaniya vysokoprochnych metallicheskich materialov na vyazkost' razrusheniya pri ploskoy deformazii (Testing of high-strength metallic materials for plain strain fracture toughness). Mir, Moskva
11. Panasyuk VV, Andreykiv AY, Kovchyk SY (1977) Metody ozenki treschinostoykosti konstrukzionnych materialov (Methods of assessment of crack growth resistance of structural materials). Naukova Dumka, Kiev
12. (1990) Metody mechanicheskich ispytaniy metallov i svarnych soedineniy. Opredelenie charakteristik treschinostoykosti (vyazkosti razrusheniya) pri staticheskom nagruzhenii (Methods of mechanical testing of metals and welded joints. Determination of crack growth resistance (fracture toughness) characteristics under static loading). SEV, Moskva
13. Shvets TM et al (1986) Akustoprozrachnye klei dlya krepleniya datchikov AE (Acoustic transparent glues for mounting AE gauges). Diagnostika i prognozirovanije razrushenija svarnykh konstruktsii 1:93–97
14. Kalemanov VI, Yaremchenko MA (1986) Osobennosti krepleniya datchikov akusticheskoy emissii (Peculiarities of AE gauges fixing). Ibid 3:86–89
15. (1990) GOST 1497-84. Metally. Metody ispytaniy na rastyazhenie, vved. 01.11. 1990 g. (Standard 1497-84. Metals. Tensile test methods. Introduced 01.11. 1990)
16. Lysak VM, Skalskiy VR, Serhiyenko OM (1994) Doslidzhennya vplyvu chvylevodu na zminu parametriv signaliv akustichnoyi emisiyi (Investigation of the influence of wave guide on the change of AE signal parameters). Fizyko-chimichna mechanika materialiv (Physicochem Mech Mater) 2:64–70
17. Skalskiy VR (2001) Okremi metodologichni zasady rozroblennya prystroyiv dlya peredavannya akustichnoyi emisiyi (Some methodological bases of development for the design of devices for acoustic emission transmission). Mashynoznavstvo 7:49–52
18. Skalskiy VR et al (1998) Prystroyi i ustanovky dlya vyznachennya trischinostiykosti konstrukziynych materialiv metodom akustichnoyi emisiyi (Devices and equipment for determination of crack growth resistance characteristics of structural materials by the method of acoustic emission). Preprint, NAN Ukrayiny, Fizyko-mechanichnyi institut, 1(1998), L'viv
19. Ermison AL, Muravin HB, Shyn VV (1986) Akustiko-emissionnye pribory i signaly (Acoustic emission devices and signals). Defektoskopia 5:3–11
20. Skalskiy VR, Demchyna BG, Karpukhin II (2000) Ruynuvannya betoniv i akustychna emisiya (Oglyad). Povidomlennya 2. Koroziya zalizobetonu. Aparaturni zasoby. AE–kontrol' ta diagnostyka budivel'nych sporud (Concrete fracture and acoustic emission (A review). Report 2. Corrosion of the reinforced concrete. Equipment. AE examination and diagnostics of building constructions). Tekhnicheskaia Diagnostika i Nerazrushyuschii kontrol (Tech Diagn Nondestr Test) 2:9–27
21. Lysak MV, Skalskiy VR (1997) Metodychnyi pidchid dlya eksperimental'noi akustyko-emisiynoi ozinky trischynotryvkosti konstrukziynych materialiv (Methodical approach for experimental acoustic-emission assessment of crack growth resistance of

structural materials). Fizyko-chimichna mechanika materialiv (Physicochem Mech Mater) 5:17–30
22. Ivanov VI (1980) Metody i apparatura kontrolya s ispol'zovaniem akusticheskoy emissii (Methods and inspection devices which use acoustic emission). Mashynostroyenie, Moskva
23. Milius PB, Hrabets I (1984) Absolyutnaya kalibrovka p'ezopreobrazovateley, ispol'zuemych dlya registrazii signalov akusticheskoy emissii (Absolute calibration of piezo-transducers, used for acoustic emission signals recording). Defektoskopia 5:27–32
24. Stryzhalo VA et al (1990) Prochnost' I akusticheskaja emissija materialov i elementov konstruktsij (Strength and acoustic emission of materials and structural elements). Naukova Dumka, Kiev
25. Vakar KB (ed) (1980) Akusticheskaya emissiya i ee primenenie dlya nerazrushayuschego kontrolya v atomnoy energetike (Acoustic emission and its application for non-destructive testing in nuclear power engineering). Atomizdat, Moskva
26. Andreykiv AE, Skalskyi VR, Lysak NV (1992) Sposob kontrolia rosta treschin v obraztsakh materialov (A test method of crack growth in material specimens). USSR Inventor's Certificate 1758545 G 01 N29/04, Bulletin No. 32, 30 Aug 1992
27. Mykytyshyn SI, Hrytsyshyn PM (1981) Sposob mekhanicheskikh ispytanij na prochnost' (A method of mechanical testing for strength). USSR Inventor's Certificate 879373, G 01 N3/00, Bulletin. No. 41, 07 Nov 1981
28. Jones MH, Brown WF (1964) Acoustic detection of crack initiation in sharply notched specimen. Mater Res and Stand 4(3):120–129
29. Greshnikov VA, Drobot YuB (1976) Akusticheskaya emissiya (Acoustic emission). Izdatel'stvo standartov, Moskva
30. Smirnov VI (1979) Ob ozenke razmerov defektov metodom akusticheskoy emissiy s poziziy mechaniki razrusheniya (On the assessment of the defect size using the method of acoustic emission from the viewpoint of fracture mechanics). Defektoskopia 2:45–50
31. Filinenko SF, Gorodiskii NI, Biriukov VS (1985) Osobennosti signalov akusticheskoy emissii pri plasticheskom deformirovanii i chrupkom razrushenii materialov (Peculiarities of acoustic emission signals under plastic deformation and brittle fracture of materials). Fiziko-chimicheskaya mechanika materialov (Physicochem Mech Mater) 6:105–106
32. Andreykiv OY et al (1990) Metodicheskie aspekty primeneniya metoda akusticheskoy emissii pri opredelenii staticheskoy treschinostoykosti materialov (Methodical aspects of application of the acoustic emission method in evaluation of static crack growth resistance of materials). Preprint, NAN Ukrayini, Fizyko-mechanichnyi instytut, 165(1990), L'viv
33. Eitzen DG, Wadley HNG (1984) Acoustic emission: establishing the fundamentals. J Res Nat Bur Stand USA 89(1):75–100
34. Breckenridge FR, Tschiegg CE, Greenspan M (1975) Acoustic emission: some application of Lamb's problem. J Acoust Soc Am 57:626–631
35. Breckenridge FR (1982) Acoustic emission transducer calibration by means of the seismic surface pulse. J Acous Emiss 1:87–94
36. Hsu N (1976) Acoustic emission simulator. USA Patent 4018084 assigned to Lockheed Aircraft Corporation, Buibouk, CA, May 1976
37. Fowler KA (1971) Acoustic emission simulation test set. Mater Res Stand 11(3):35–38
38. (1971) Now hear this. A newsletter on acoustic emission, vol 1(3). Dunegan/Endevco
39. Jones M, Green R, Hsu N (1983) Comparison of simulated acoustic emission sources. Proc Ultrasonic Int
40. Williams JH, Kahn EB, Lee SS (1983) Effect of specimen resonances on acoustic-ultrasonic testing. Mater Eval 13:1502–1510
41. Katsuyama K, Sato K (1985) Influence of acoustic emission source location on acoustic emission waveform. Saiko to khoan 31(1):2–10
42. Andreykiv OY et al (1993) The contribution of Rayleigh waves to the acoustic field arising from internal defect growth. Mater Sci 29(2):115-120

43. Skalskyi VR, Zazuliak VA, Kovchyk SY, Rybytskyi IB (1994) Sposib kalibrovky akustyko-emisiynoho vymiruval'noho traktu (A calibration method of acoustic emission measuring channel). Patent of Ukraine No. 2895, G01 N 29/14, Bulletin. No.5-1 26 Dec 1994
44. Viktorov NA (1966) Fizicheskie osnovy primeneniya ul'trazvukovych voln Releya i Lemba v technike (Physical bases of ultrasonic Raleigh and Lamb waves application in engineering). Nauka, Moskva
45. Wadley HNG, Scrubi CB, Speake JU (1980) Acoustic emission for physical examination of metals. Int Met Rev 25(2):41–64
46. Skalskyi VR, Andreikiv AY (2003) Sposib imituvannia akustychnoji emisii na objekti kontrolu (A method of imitation of acoustic emission in the inspected object). Patent of Ukraine No. 54963A, G01N29/14, G01N3/00, Bulletin No. 3, 17 Mar 2003
47. (1981) Mechanika razrusheniya. Bystroe razrushenie, ostanovka treschin (Fracture Mechanics. Rapid fracture, crack arrest). In: Goldstain (ed) Mechanika. Novoe v zarubezhnoy nauke (Mechanics. Novelty in foreign science), is 25. Mir, Moskva, pp 199-221
48. Obuhivskyi OI Rasklinivanie kvadratnogo obrazza s bokovoy treschinoy (Wedging of a square specimen with an edge crack). Fiziko-chimicheskaya mechanika materialov (Physicochem Mech Mater) 3:111-112
49. Likhtman VI, Rebinder PA, Karpenko GV (1954) Vliyanie poverchnostno-aktivnoy sredy na prozessy deformazii metallov (Influence of surface-active medium on deformation processes of metals). Izd-wo AN SSSR, Moskva
50. Bukhalo OP (1997) Obrazzovyy impul'snyy stochasticheskiy signal–primenenie, vosproizvedenie, attestaziya (A standard pulse stochastic signal-application, reproduction, certification). Izmeritelnaya tekhnika (Meas Equip) 6:24–33
51. Andreykiv OY et al (1993) Spektral'nyy analiz akusticheskoy emissii rastuschey treschiny (Spectral analysis of acoustic emission of a growing crack). Tekhnicheskaja diagnostika i nerazrushajuschii kontrol (Tech Diagn Nondestr Test) 1:75–84
52. Greshnikov VA, Braginskyi AP (1980) Ob analize signalov akusticheskoy emissii (On the analysis of acoustic emission signals). Defektoskopia 5:101–106
53. Batuyev VT et al (1973) Spektral'nyy analiz EVH na ploschadke tekuchesti (Spectral analysis of stress wave emission at the yield area). In: Tezisy dokladov nauch.-techn. konf. "Herazrushayuschiy kontrol' kachestva", Hovosibirsk, 1973 (Theses reports conf. "Nondestructive testing of quality", Novosibirsk, 1973)
54. Muravin G, Lezvinskaya LM (1982) Issledovanie spektral'noy plotnosti signala AE (Investigation of spectral density of AE signal). Defektoskopia 7:10–15
55. Acquaviva CJ (1980) Interlaboratory comparison of crack emission spectra. NDT Int 5:230–234
56. Kline R, Hartman WF (1976) Frequency analysis of acoustic emission signals. In: International conference on mechanical behavior of materials, pp 1631–1635
57. Vainberg VE, Kats MS, Purych EI (1981) Vliyanie razmera obrazza na chastotnyy spektr akusticheskoy emissii (Influence of specimen size on the frequency spectrum of acoustic emission). Defektoskopia 4:110–112
58. Gorbunov AI, Lykov YuI (1986) Vliyanie amplitudno-chastotnych charakteristik ob'ekta na spektral'nye charakteristiki signalov AE (Influence of amplitude frequency characteristics of an object on spectrum characteristics of AE signals). Ibid 9:39–45
59. Muravin G, YaV Simkin, Merman AI (1989) Identifikaziya mechanizma razrusheniya materialov metodami spektral'nogo analiza signalov akusticheskoy emissii (Identification of the fracture mechanism by the method of spectral analysis of acoustic emission signals). Ibid 4:8–15
60. Fleischman P (1975) A spectrum analysis of acoustic emission. Non-Destr Test 8(5):241–244
61. Greham JZ, Alera G (1974) Spectrum analysis of acoustic emission. Mater Eval 2:31–37
62. Stephens RWB, Pollock AA (1971) Waveform and frequency spectra of acoustic emission. J Acoust Soc Amer 50(3):904–910
63. Lysak MV (1994) Acoustic emission during jumps in subcritical growth of crack in three-dimensional bodies. Eng Fract Mech 47(6):873–879

64. Kucherov IY et al (1985) Issledovanie chuvstvitel'nosti i diagramm napravlennosti priemnikov akusticheskoy emissii (Investigation of sensitivity and directional diagrams of the acoustic emission receivers). Diagnostika i prognozirovanije razrushenija svarnykh konstruktsii 1:53–58
65. Kishi T, Okita T (1984) Ozenka tipa razrusheniya po diagramme napravlennosti izlucheniya v signalach akusticheskoy emissii (Evaluation of the fracture type by the directional diagram of irradiation in the acoustic emission signals). Nihon kindziuku gakkaisi 48(9):911–917
66. Scruby CB, Wadley HNG, Rusbridge KL (1983) Origin of acoustic emission in Al–Zn–Mg alloys. Mater Sci Eng 59(2):169–183
67. Andreykiv AY, Lysak NV, Serhiyenko ON (1990, 1991) Modelirovanie prozessov lokal'nogo razrusheniya, soprovozhdayuschegosya akusticheskoy emissiey v materialach i izdeliyach (Modelling of the process of local fracture, assisted by acoustic emission in materials and products). Tekhnicheskaja diagnostika i nerazrushajuschii control (Tech Diagn Nondestr Test) 1:9–20, 1:59–65
68. Kishi T (1985) Acoustic emission source characterization and its application to microcracking. Z Metallk 76(7):512–515
69. Lysak NV, Skalskiy VR (1993) O napravlennosti akustiko-emissionnogo izlucheniya pri razrushenii materialov i ee prakticheskoe primenenie (On direction of acoustic emission irradiation during material fracture and its practical application). Tekhnicheskaja diagnostika I nerazrushajuschii control (Tech Diagn Nondestr Test) 3:22–32
70. Achenbach JD, Harris JC (1979) Acoustic emission from a brief crack propagation event. Trans ASME, J Appl Mech, Ser E 46(1):107–112, 187–221
71. Wadley HNG, Scruby CB (1983) Elastic wave radiation from cleavage crack extension. Int J Fract 23:111–128
72. YaU Saatov, Bykovtsev AS, Khamidov LA (1985) Seysmologicheskie zadachi mechaniki razrusheniya (Seismic problems of fracture mechanics). Mekhnat, Tashkent
73. Drobot YuB, Lazariev AM (1987) Herazrushayuschiy kontrol' ustalostnych treschin akustiko-emissionnym metodom (Nondestructive testing of fatigue cracks by an AE method). Izdatel'stvo standartov, Moskva
74. Andreykiv OYe et al (2000) Deyaki metodichni zasnovki ozinki poshkodzhenosti virobiv za signalami akustichnoyi emisiyi (Some methodical pre-conditions of estimation of damages of products by the signals of acoustic emission). Fiziko-chimichna mechanika materialiv (Physicochem Mech Mater) 2:83–92
75. Nesmashniy EV et al (1984) O svyazi amplitudy signala AE s prirascheniem ploschadi treschiny (On the relation of the amplitude of AE signals with increment of the crack area). In: Sbornik tezisov i dokladov I Vsesoyuznoy konferenzii "Akusticheskaya emissiya materialov i konstrukziy" (Theses of reports 1st all-union conference. "Acoustic emission of materials and structures", 11–13 Sept 1984, Rostov upon-Don, 1984), vol 1. Rostov-na-Donu
76. Aleksieyev IG, Kudrya AV, Shtremel MA (1994) Parametry akusticheskoy emissii, nesuschie informaziyu ob edinichnoy chrupkoy treschine (Acoustic emission parameters, containing information about a single brittle crack). Defektoskopia 12:29–34
77. Harris JG, Pott J (1984) Surface motion excited by acoustic emission from a buried crack. Trans ASME J Appl Mech 51(1):77–83
78. Kolesnikov AE (1982) Ul'trazvukovye izmereniya (Supersonic measuring). Izdatel'stvo standartov, Moskva
79. Melnychenko ZM, Shvets TM, Podychevska SA, Kharchenko LF (1983) Kley (Glue). USSR Inventor's Certificate, G1014875, Bul. No. 16
80. Appasov AM (1998) Ustroystvo dlya priema signalov akusticheskoy emissii (Equipment for receiving acoustic emission signals). Zavodskaya Laboratoria 10:25–29
81. (1972) Acoustic emission. ASTM Special Technical Publication 505. Baltimor
82. Andreikiv OY, Skalskyi VR, Lysak MV (1994) Sposib kontrolu rostu trischyn u zrazkakh materialiv (A method of checking the growth of cracks in the material specimens). Patent of Ukraine N2914, MPK: G01N29/14, Bul. 5-1, 26 Dec 1994

83. Sharp R (ed) Metody nerazrushayuschich ispytaniy. Fizicheskie osnovy, prakticheskie primeneniya, perspektivy razvitiya (Methods of non-destructive testing. Physical bases, practical application, prospects of development). Mir, Moskva
84. Kiriakin AV, Zheleznaja IL (1984) Akusticheskaya diagnostika uzlov i blokov REA (Acoustic diagnostics of units and blocks of electronics). Radio i sviaz, Moskva
85. Kollacott R (1989) Diagnostika povrezhdeniy (Damage diagnostics) (trans Babajevskyi PG). Mir, Moskva
86. Kisi T (1976) Acoustic emission. Kindzoku Dzaire 165:107–113
87. Birchon D (1979) Cries of stress. Spectrum 165:5–8
88. Shyn VV, Dementiev AN (1987) Metodicheskie osnovy akustiko-emissionnogo kontrolya svarnych soedineniy gazoprovodov (Methodical bases of acoustic-emission control of welded joints in gas pipelines). Diagnostika i prognozirovanije razrushenija svarnykh konstruktsii 5:46–52
89. Vehaviolos SJ (1975) SWE: a tool for non-destructive testing. Tooling Prod 41(3):52–53
90. Stern R (1972) Experimental techniques in acoustic emission detection systems. In: Ultrasonics symposium, Boston, 1972, Catalogue 372 CHO 708-8SU. IEEE
91. Arrington M (1981) An introduction to the technology and applications of acoustic emission. Tin cries-but most materials talk. Phys Technol 12:16–23
92. Dunegan HL, Tatro CA (1971) Acoustic emission effect during mechanical deformation. In: Bunshan RF (ed) Techniques of metals research, vol 5, part 2 (Chap. 12). Interscience Publications, New York, pp 273–312
93. Nakamura I (1971) Acoustic emission monitoring system for detection of cracks in a complex structure. Mater Eval 29(1):8–12
94. Ruby D (1980) Emission acoustique et conrole nondesructif. CET HEDEC Revue 17 (2):13-19, 205–231
95. (1995) MISTRAS 2001. AEDSP—32/16. User's manual. Rev. 1. PAC Part Number 6300-1000
96. Takahashi H et al (1981) Acoustic-emission crack monitoring in fracture-toughness tests for AISI 4340 and SA533B steels. Exp Mech 21(3):89–99